Draft version December 9, 2016
Preprint typeset using LaTeX style emulateapj v. 5/2/11

arXiv:1612.02163v2 [astro-ph.SR] 8 Dec 2016

GENERAL MODEL FOR LIGHT CURVES OF CHROMOSPHERICALLY ACTIVE BINARY STARS

L. Jetsu
Department of Physics, P.O. Box 64, FI-00014 University of Helsinki, Finland

G.W. Henry
Center of Excellence in Information Systems, Tennessee State University, 3500 John A. Merritt Blvd., Box 9501, Nashville, TN 37209, USA

J. Lehtinen
Max-Planck-Institut für Sonnensystemforschung, Justus-von-Liebig-Weg 3, 37077 Göttingen, Germany
Draft version December 9, 2016

ABSTRACT

The starspots on the surface of many chromospherically active binary stars concentrate on long–lived active longitudes separated by 180 degrees. The activity shifts between these two longitudes, the "flip–flop" events, have been observed in single stars like FK Comae and binary stars like σ Geminorum. Recently, interferometry has revealed that ellipticity may at least partly explain the "flip–flop" events in σ Geminorum. This idea was supported by the double peaked shape of the long–term mean light curve of this star. Here, we show that the long–term mean light curves of fourteen chromospherically active binaries follow a general model which explains the connection between orbital motion, starspot distribution changes, ellipticity and "flip–flop" events. Surface differential rotation is probably weak in these stars, because the interference of two constant period waves may explain the observed light curve changes. These two constant periods are the active longitude period ($P_{\rm act}$) and the orbital period ($P_{\rm orb}$). We also show how to apply the same model to single stars, where only the value of $P_{\rm act}$ is known. Finally, we present a tentative interference hypothesis about the origin of magnetic fields in all spectral types of stars.

Subject headings: techniques: photometric – methods: data analysis – stars: binary – stars: activity

1. INTRODUCTION

An ancient Egyptian calendar of lucky and unlucky days, the Cairo Calendar, is the oldest preserved historical document of the discovery of a variable star, Algol (Porceddu et al. 2008; Jetsu et al. 2013; Jetsu & Porceddu 2015). Today, the General Catalogue of Variable Stars contains nearly 50,000 stars. There are numerous classes of variable stars and the classification criteria are constantly updated (Samus et al. 1997). Different classes have their own typical light curves (Drake et al. 2014). One class of variable stars is called the Chromospherically Active Binary Stars (hereafter CABS). The third catalogue of CABS lists 409 such binaries (Eker et al. 2008).

In his review of starspots, Strassmeier (2009) wrote that the "starspot hypothesis" was first presented by a French astronomer Ismael Boulliau (1605–1694) to explain the variability of Mira. This star, also known as *o* Ceti, was the first variable star discovered by "modern" astronomers in 1596 (David Fabricius, 1564–1617). Boulliau's hypothesis was unfortunately not true, because pulsations cause the variability of Mira. According to Strassmeier (2009), the first observations of starspots were made by Kron (1947) in the light curves of four eclipsing binaries. The presence of this phenomenon in the light curves of active stars was firmly established later by Hoffmeister (1965); Chugainov (1966); Catalano & Rodonò (1967); Hall (1972).

Unlike the longitudinally evenly distributed sunspots in the Sun, the starspots in active single (e.g. Jetsu et al. 1993, FK Com) or binary (e.g. Jetsu 1996, σ Gem) stars concentrate on long–lived active longitudes and seem to undergo shifts of about 180 degrees in longitude. The presence of this "flip–flop" phenomenon in the CABS, σ Gem, was questioned by Roettenbacher et al. (2015). Their interferometric observations revealed that ellipticity of σ Gem may explain the stability of the two minima in the long–term mean light curve (hereafter MLC). Recently, Siltala et al. (2016) reported that another CABS, BM CVn, has a sinusoidal MLC with an amplitude of $0.^{\rm m}042$. Ellipticity fails to explain the MLC shape of BM CVn. Here, we study the light curves of fourteen CABS. Our sample includes the light curves of the two above mentioned CABS, σ Gem and BM CVn.

We use the following abbreviations

CABS = Chromospherically Active Binary Star

MLC = Mean Light Curve

CPS = Continuous Period Search

A = More active CABS member

B = Other CABS member

Aa = A in front of B epoch

lauri.jetsu@helsinki.fi

Ac = B in front of A epoch

Ab = Mid epoch between Aa and Ac

Ad = Mid epoch between Ac and Aa

S1 = Larger starspot on A

S2 = Smaller starspot on A

S1f = S1 visibility maximum at Aa & No S2

S1b = S1 visibility maximum at Ac & No S2

S12fb = S1 visibility maximum & S2 unseen at Aa

S12bf = S1 unseen & S2 visibility maximum at Aa

The meaning of the last ten abbreviations is explained in greater detail in Sect. 6.1.

2. OBSERVATIONS

Our differential standard Johnson V photometric observations were made with the T3 0.4m automated photoelectric telescope (APT) at Fairborn Observatory in Arizona. The information of our photometry of fourteen CABS is summarized in the seven first columns of Table 1. The accuracy of the differential V magnitudes is approximately $0.^{\rm m}006$. Henry (1999) and Fekel & Henry (2005) have described the operation of the T3 0.4 m APT and photometric data reduction procedures in greater detail.

3. MLC ANALYSIS

The original data are the differential V magnitude observations $m_i = m(t_i)$, where t_i is the observing time. The time points are transformed into phases $\phi_i = \mathrm{FRAC}[(t_i - t_0)/P_{\rm orb}]$, where FRAC removes the integral part of its argument, i.e. the number of full orbital rounds $P_{\rm orb}$ completed after t_0. The $P_{\rm orb}$ and t_0 values of each CABS (Eker et al. 2008) are given in Table 1. The m_i observations are binned in phase, using $N = 20$ evenly spaced bins, where the limits of the j:th bin are $(j-1)/N \leq \phi_i < j/N$. A bin must contain at least two m_i values. The binned data for the n_j values of m_i in the j:th bin are $x_j = (j/N) - 0.25$, $y_j = n_j^{-1} \sum_{i=1}^{n_j} m_i$, $\sigma_j = n_j^{-1/2}[n_j^{-1} \sum_{i=1}^{n_j}(m_i - y_j)^2]^{1/2} = n_j^{-1}[\sum_{i=1}^{n_j}(m_i - y_j)^2]^{1/2}$.

The model for these data is

$$g(x, \bar{\beta}) = a_0 + \sum_{k=1}^{K} a_i \cos(kx) + b_i \sin(kx), \qquad (1)$$

where $\bar{\beta} = [a_0, a_1, ..., a_K, b_1, ..., b_K]$ are the free parameters. Note that the model is simply $g(t, \bar{\beta}) = a_0$, if $K = 0$. The model residuals $\epsilon_j = y_j - g(x_j, \bar{\beta})$ give $\chi^2(\bar{y}, \bar{\beta}) = \sum_{j=1}^{N} w_j \epsilon_j$, where $w_j = \sigma_j^{-2}$.

The main question is, do these data contain a periodic signal? And if so, what is the correct order K for the model of this signal? We solve this problem, as Lehtinen et al. (2011) did, by computing the Bayesian information criterion parameter

$$R_{\rm BIC} = 2n \, \ln\lambda(\bar{y}, \bar{\beta}) + (5K + 1) \, \ln \, n, \qquad (2)$$

where $\lambda(\bar{y}, \bar{\beta}) = \chi^2(\bar{y}, \bar{\beta})[\sum_{j=1}^{N} w_j]^1$. The best modelling order K for the data is the value of the order that minimizes $R_{\rm BIC}$. We test the values $K = 0, 1$ and 2 for the binned data of each CABS. The best K value for the MLC of all data of each star, and the peak to peak amplitude $A_{\rm All}$ of this MLC, are given in Table 1. The periodic MLC phenomenon is present in all fourteen CABS (i.e. $K \geq 1$).

We divide the data in two parts in our Figs. 1 – 14. This shows, if MLC changes. The 1st and 2nd parts are before and after $t_1 + \Delta T/2$, respectively. The order K of the MLC model for the 1st and 2nd part of data is fixed to the K value obtained for all data. However, the amplitudes of these MLC models, A_1 and A_2, are determined separately from a fit to the binned data of the 1st and 2nd part of data. We use the notation ΔA for the maximum difference between the three amplitudes $A_{\rm All}$, A_1 and A_2.

The orbital ephemeris epoch (t_0), the orbital period (P_0), the eccentricity (e) and the spectral type of A member of CABS information in Tables 1 and 2 is from Eker et al. (2008, third catalogue of CABS). The original references for this information are given in Sect. 4, where the results for each individual star are discussed separately. We use the radial velocity maximum epochs of Table 2 (Ab epochs) to compute the orbital phases from

$$\phi_{\rm orb} = \mathrm{FRAC}[(t - t_0)/P_{\rm orb}], \qquad (3)$$

where t_0 is the Ab epoch given in Table 2.

4. MLC ANALYSIS RESULTS

Here, we describe the MLC of each individual CABS and give the original references for their physical parameters in Tables 1 and 2.

4.1. *MLC of DM UMa*

The high amplitude, $A_{\rm All} = 0.^{\rm m}071$, sinusoidal MLC of DM UMa remains nearly unchanged between $0.4 < \phi_{\rm orb} < 0.6$ (Figs. 1ceg). The largest MLC changes occur between Aa $\equiv -0.25 < \phi_{\rm orb} < 0.25 \equiv$ Ac. MLC level, shape and phase are nearly stable. MLC amplitude changes are small ($\Delta A = 0.^{\rm m}013$). MLC minimum coincides with Aa (Crampton et al. 1979; Glebocki & Stawikowski 1995; Barrado y Navascues et al. 1998; Hatzes 1998, $P_{\rm orb}$, t_0, e, Sp-type of member A).

4.2. *MLC of XX Tri*

The sinusoidal MLC of XX Tri has an extremely high amplitude of $A_{\rm All} = 0.^{\rm m}136$. This variation increases to $A_1 = 0.^{\rm m}233$ during the 1st part of data, and then decreases to $A_2 = 0.^{\rm m}025$ in the 2nd part. Despite of these dramatic changes, MLC phase remains stable. MLC minimum and maximum phases coincide with Aa and Ac epochs (Bopp et al. 1993; Strassmeier & Olah 1992; Strassmeier 1999, $P_{\rm orb}$, t_0, e, Sp-type of member A). Note the minor MLC dips at $\phi_{\rm orb} = 0.25$ and 0.75 in Fig. 2g which will be discussed later in Sect. 6.1.4.

4.3. *MLC of EL Eri*

EL Eri has a sinusoidal MLC with an amplitude of $A_{\rm All} = 0.^{\rm m}048$ (Fig. 3c). MLC shape, amplitude and

Table 1
CABS sample.

Variable		Comparison	Beg	End	ΔT [y]	n	$P_{\rm orb}$ [d]	t_0 [HJD − 2400000]	e	K	$A_{\rm All}$ [mag]
DM UMa	SAO 15334	HD 95362	29.10.1988	13.6.2015	26.6	1915	7.492	43881.4 [*a*]	0	1	0.071
XX Tri	HD 12545	HD 12478	7.10.1990	13.2.2015	24.4	1962	23.96924	47814.315 [*a*]	0	1	0.136
EL Eri	HD 19754	HD 19421	19.10.1990	11.2.2015	24.3	1642	48.263	44419.9 [*b*]	0.1	1	0.048
V711 Tau	HD 22468	HD 22484	13.11.1987	11.3.2015	27.3	2293	2.83774	51142.943 [*c*]	0	2	0.030
EI Eri	HD 26337	HD 26409	11.1.1988	7.3.2015	27.2	2268	1.947227	46091.052 [*a*]	0	2	0.017
V1149 Ori	HD 37824	HD 38309	13.9.1988	28.3.2015	26.5	2274	53.57465	48625.022 [*a*]	0	1	0.050
σ Gem	HD 62044	HD 60318	21.11.1987	1.5.2015	27.4	2984	19.60447	47227.15 [*d*]	0.012	2	0.039
FG Uma	HD 89546	HD 90400	15.3.1992	11.6.2015	23.2	3145	21.35957	49297.702 [*a*]	0	2	0.045
HU Vir	HD 106225	HD 105796	6.4.1990	15.6.2015	25.2	2062	10.387552	49993.195 [*b*]	0.0093	2	0.136
BM CVn	HD 116204	HD 116010	6.4.1990	17.6.2015	25.2	2917	20.6252	45251.62 [*a*]	0	1	0.040
V478 Lyr	HD 178450	HD 177878	14.11.1987	21.6.2015	27.6	2641	2.1305140	45939.801 [*a*]	0	2	0.010
V1762 Cyg	HD 179094	HD177483	25.4.1988	21.6.2015	27.2	2526	28.58973	31043.408 [*a*]	0	2	0.031
HK Lac	HD 209813	HD 210731	30.4.1988	21.6.2015	27.1	2454	24.4284	40017.17 [*b*]	0.01	1	0.089
II Peg	HD 224085	HD 224930	16.11.1987	23.1.2015	27.2	2049	6.724333	49582.9268 [*e*]	0	1	0.064

Note. — Variable (Cols 1-2: Variable designation and HD or SAO number), comparison star (Col 3: SAO- or HD-number), first and last observing date (Cols 4-5: Beg and End), time span and number of observations (Cols 6-7: [ΔT] = y and n), orbital period, epoch and eccentricity (Cols 8-10: $P_{\rm orb}$ = d, t_0 and e, epoch types: [*a*]= Radial velocity maximum, [*b*]= Periastron, [*c*]= Cool in front, [*d*]= Primary in front, [*e*]= Primary behind), MLC order and amplitude (Cols 11-12: K and [$A_{\rm All}$] = mag).

Table 2
CABS sample.

Variable		Sp-type of A	Aa	Ab	Ac
DM UMa	SB1	K0–1 IV–III	43879.527	43881.400	43883.273
XX Tri	SB1	K0 III	47808.323	47814.315	47820.307
EL Eri	SB1	G8 III–IV	44419.966	44432.032	44444.097
V711 Tau	SB2	K1 IV	51142.943	51143.652	51144.362
EI Eri	SB1	G5 IV	46090.565	46091.052	46091.539
V1149 Ori	SB1	K0 III	48611.628	48625.022	48638.416
σ Gem	SB1	K1 III	47227.150	47232.051	47236.952
FG Uma	SB1	G9 III	49292.362	49297.702	49303.042
HU Vir	SB1	K2 III	49993.403	49996.000	49998.597
BM CVn	SB1	G8 III	45246.464	45251.620	45256.776
V478 Lyr	SB1	G8 V	45939.268	45939.801	45940.334
V1762 Cyg	SB2	K2 IV–III	31036.261	31043.408	31050.555
HK Lac	SB1	K0 III	40011.066	40017.173	40023.281
II Peg	SB1	K2 V	49579.565	49581.246	49582.927

Note. — Variable (Col. 1), Single-lined (SB1) or double-lined (SB2), Sp-type of member A, epochs Aa, Ab and Ac [HJD-2400000] (Cols 2-6)

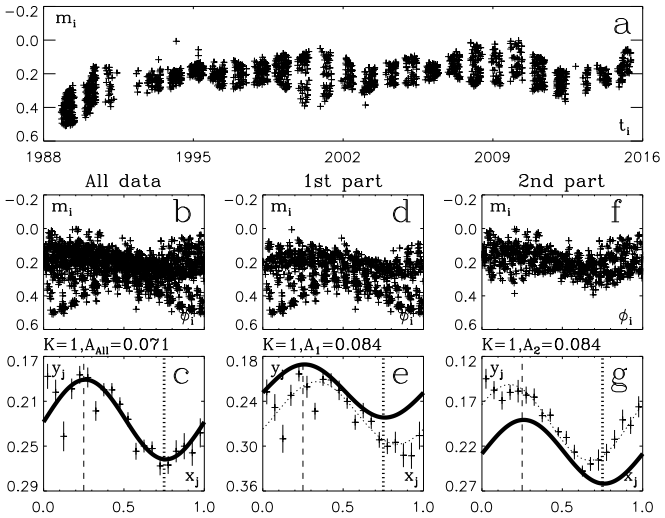

Figure 1. DM UMa, **(a)** All data: V magnitudes (crosses) versus time. **(b)** All data: V magnitudes (crosses) versus orbital phase. **(c)** All data: Binned magnitudes (crosses with error bars), MLC (thick continuous line), order (K) and amplitude ($A_{\rm All}$). Epoch Aa (thick dotted vertical line) and epoch Ac (thin dashed vertical line). **(d)** 1st part of data: V magnitudes (crosses) versus orbital phase. **(e)** 1st part of data: Binned magnitudes (crosses with error bars), MLC (thin dashed line), order (K), amplitude (A_1) and MLC of all data (thick line from "a"). Epoch Aa (thick dotted vertical line) and epoch Ac (thin dashed vertical line). **(fg)** 2nd part of data: otherwise as in "de"

phase remain quite stable ($\Delta A = 0.^{\rm m}018$), despite of the large mean level changes between 1st and 2nd part (Figs 3c–g). The Aa and Ac epochs nearly coincide with MLC maximum and minimum (Balona 1987; Fekel et al. 1986, $P_{\rm orb}$, t_0, e, Sp-type of member A).

4.4. *MLC of V711 Tau*

The double peaked MLC of V711 Tau has a low amplitude (Fig. 4: $A_{\rm All} = 0.^{\rm m}030$). This amplitude remains quite stable (Figs. 4ceg: $\Delta A = 0.^{\rm m}012$), regardless of the changes in the mean level (Figs. 4df). MLC primary minimum phase $\phi_{\rm orb} = 0.25$ does not shift, but the secondary minimum $\phi_{\rm orb} = 0.8$ in the 1st part shifts to 0.7 in the 2nd part. The epochs of Ac and Aa coincide with the MLC primary and secondary minima (Fekel 1983; Donati et al. 1992; García-Alvarez et al. 2003, $P_{\rm orb}$, t_0, e, [Sp-type of member A). However, the interpretation this MLC may be more complicated, because the hotter member B (G5 IV) could also influence MLC (Fekel 1983; García-Alvarez et al. 2003).

4.5. *MLC of EI Eri*

EI Eri has a very stable low amplitude double peaked MLC (Fig. 5a: $A_{\rm All} = 0.^{\rm m}017$). MLC mean and amplitude do not change. Only minor MLC changes occur in the interval $0.25 < \phi_{\rm orb} < 0.75$. MLC primary minimum at $\phi_{\rm orb} = 0.65$ in the 1st part shifts to $\phi_{\rm orb} = 0.20$ in the 2nd part. Epochs of Ac and Aa occur about $\Delta\phi_{\rm orb} = 0.05$ after MLC secondary and primary minima (Fekel et al. 1986, 1987; Strassmeier 1990; Cutispoto 1995, $P_{\rm orb}$, t_0, e, Sp-type of member A).

4.6. *MLC of V1149 Ori*

V1149 Ori has a sinusoidal MLC with an amplitude of $A_{\rm All} = 0.^{\rm m}050$ (Fig. 6c). MLC amplitude, shape and minimum are stable (Figs. 6ceg: $\Delta A = 0.^{\rm m}012$), although MLC mean changes are large (Figs. 6df).

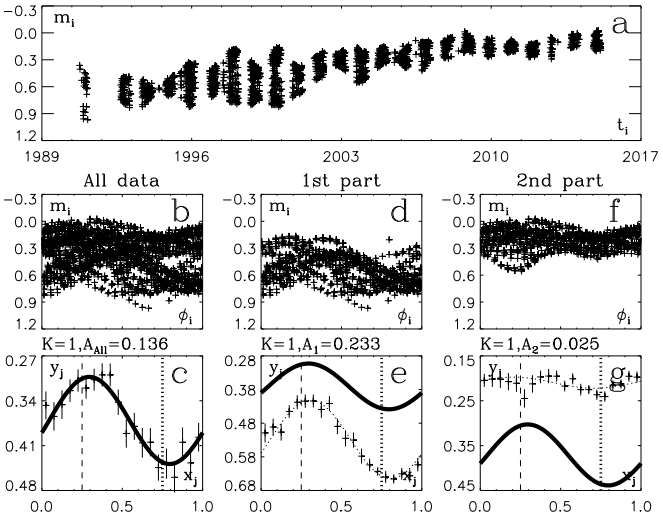

Figure 2. XX Tri , otherwise as in Fig. 1.

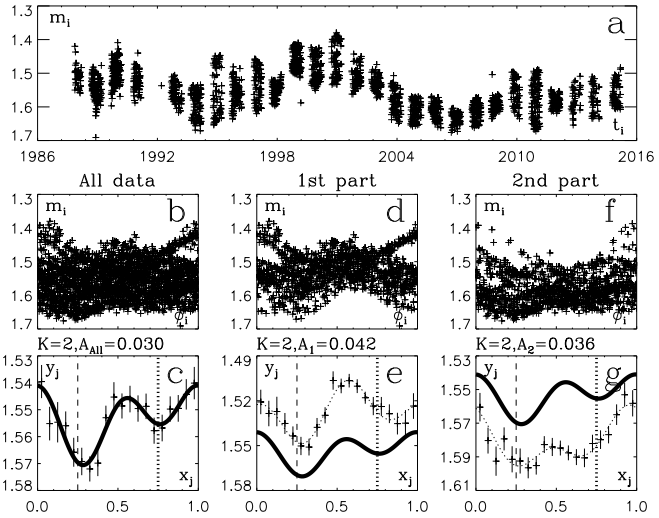

Figure 4. V711 Tau, otherwise as in Fig. 1.

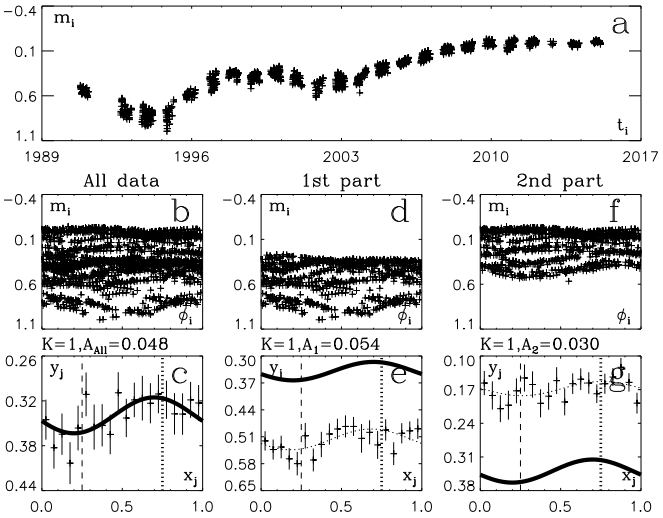

Figure 3. EL Eri, otherwise as in Fig. 1.

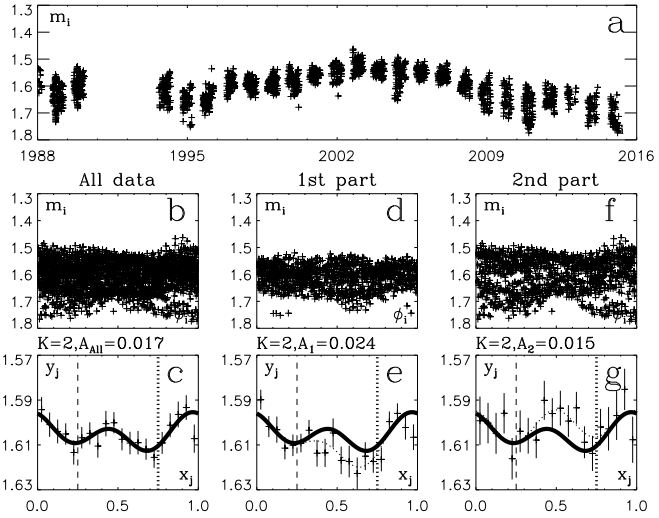

Figure 5. EI Eri, otherwise as in Fig. 1.

Epochs of Ac and Aa occur about $\Delta\phi_{\rm orb} = 0.15$ before MLC maximum and minimum (Hall et al. 1991; Fekel & Henry 2005, $P_{\rm orb}$, t_0, e, Sp-type of member A). Note the MLC dip at about $\phi_{\rm orb} = 0.75$ in Figs. 6ceg, which will be discussed later in Sect. 6.1.4.

4.7. *MLC of σ Gem*

σ Gem has a stable double peaked MLC with an amplitude of $A_{\rm All} = 0.^{\rm m}039$ (Fig. 7: $\Delta A = 0.^{\rm m}011$). MLC mean, amplitude, minimum and maximum do not change. Small changes are seen only in the interval $0.50 < \phi_{\rm orb} < 0.75$. MLC primary and secondary minima coincide with the Ac and Aa epochs (Strassmeier et al. 1988; Bopp & Dempsey 1989; Duemmler et al. 1997, $P_{\rm orb}$, t_0, e, Sp-type of member A).

4.8. *MLC of FG UMa*

FG UMa has a stable second order MLC ($K = 2$). MLC amplitude is about constant ($\Delta A = 0.^{\rm m}010$). The double peaked shape and phase of this MLC is the same in Figs. 8ceg, although the mean levels of the 1st and 2nd part of the m_i data are different in Figs. 8df. The activity level changes alter only MLC mean, but not MLC shape, minimum, maximum or amplitude. MLC primary and secondary minima nearly coincide with Ac and Aa (Fekel et al. 2002, $P_{\rm orb}$, t_0, e, Sp-type of member A).

4.9. *MLC of HU Vir*

HU Vir has a high amplitude, $A_{\rm All} = 0.^{\rm m}136$, second order MLC with a nearly sinusoidal shape (Fig. 9c). MLC amplitude is smaller in 1st part, $A_1 = 0.074$, and increases to an extreme value $A_2 = 0.198$ in the 2nd part. The Ac epoch is close to MLC primary minimum, while Aa is close to a weak secondary minimum which is more clearly visible in Fig. 9g of the 2nd part (Cutispoto 1993; Fekel et al. 1999, $P_{\rm orb}$, t_0, e, Sp-type of member A).

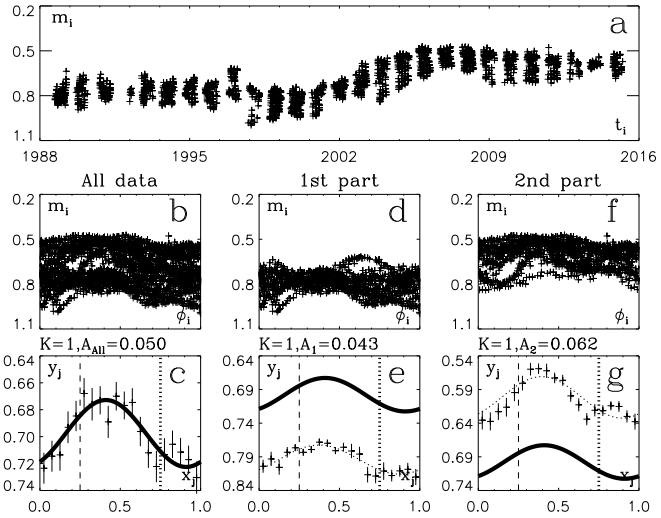

Figure 6. V1149 Ori, otherwise as in Fig. 1.

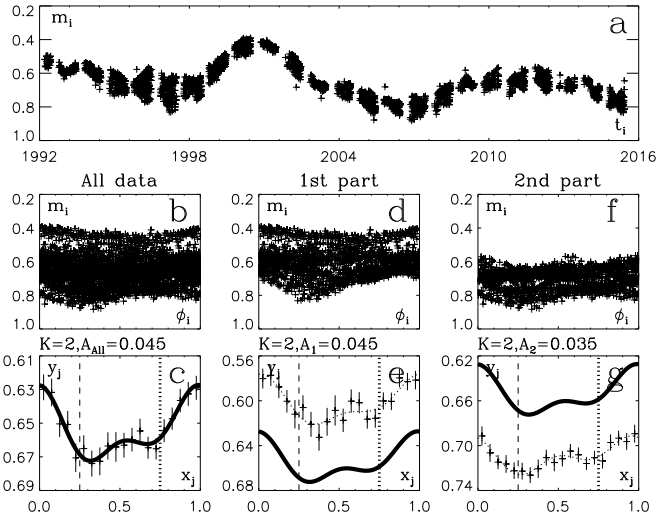

Figure 8. FG UMa , otherwise as in Fig. 1.

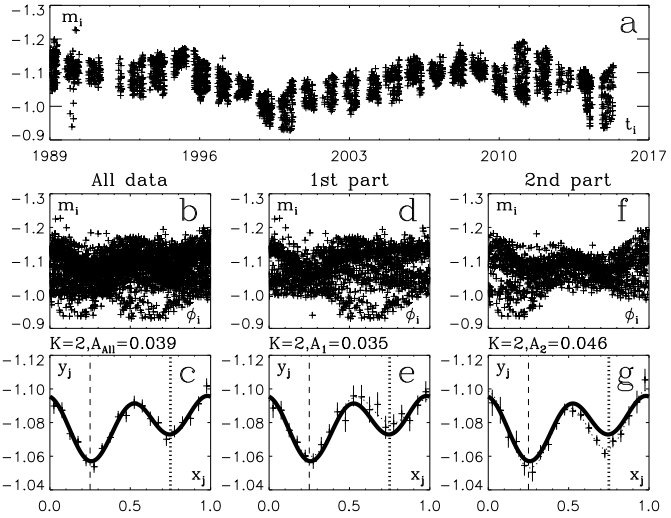

Figure 7. σ Gem , otherwise as in Fig. 1.

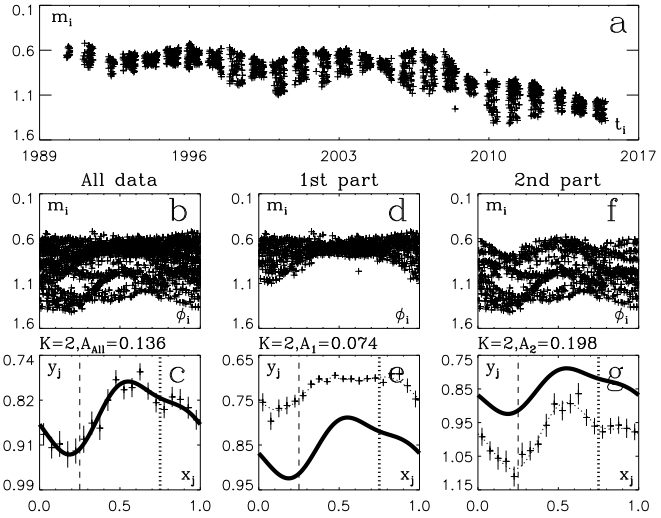

Figure 9. HU Vir, otherwise as in Fig. 1.

4.10. *MLC of BM CVn*

BM CVn has a stable sinusoidal MLC (Figs. 10cdg). Small MLC changes occur in the $-0.10 < \phi_{\rm orb} < 0.40$ interval, but none in the $0.40 < \phi_{\rm orb} < 0.90$ interval. Aa and Ac epochs are about $\Delta\phi_{\rm orb} = 0.15$ before MLC minimum and maximum (Griffin & Fekel 1988; Koen & Eyer 2002, $P_{\rm orb}$, t_0, e, Sp-type of member A).

4.11. *MLC of V478 Lyr*

MLC of V478 Lyr is double peaked and has a very low amplitude of $A_{\rm All} = 0.^{\rm m}010$. MLC shape and amplitude do not change a lot (Figs. 11ceg: $\Delta A = 0.^{\rm m}015$), although the activity levels do (Figs. 11df). MLC primary minimum at $\phi_{\rm orb} = 0.10$ in the 1st part shifts to $\phi_{\rm orb} = 0.65$ in the 2nd part. The Ac and Aa epochs occur about $\Delta\phi_{\rm orb} = 0.1$ after MLC secondary and primary minima (Griffin & Fekel 1988, $P_{\rm orb}$, t_0, e, Sp-type of member A).

4.12. *MLC of V1762 Cyg*

V1762 Cyg has a double peaked MLC with $A_{\rm All} = 0.^{\rm m}031$ (Fig. 12c). MLC mean is stable but MLC amplitude changes occur ($\Delta A = 0.^{\rm m}030$). The MLC primary minimum at $\phi_{\rm orb} \approx 0.4$ in the 1st part shifts to $\phi_{\rm orb} = 0.9$ in the 2nd part (Figs. 12ceg). MLC is stable only in the short interval $0.00 < \phi_{\rm orb} < 0.15$. The Ac epoch occurs about $\Delta\phi_{\rm orb} = 0.15$ before MLC primary minimum, while Aa remains close to MLC maximum (Osten & Saar 1998, $P_{\rm orb}$, t_0, e, SP-type of A). Note the switch of MLC minimum and maximum in Figs. 12ef between the 1st and 2nd part data. This switch will be discussed in Sect. 6.1.5.

4.13. *MLC of HK Lac*

HK Lac has a high amplitude, $A_{\rm All} = 0.^{\rm m}089$, sinusoidal MLC which remains stable at $0.00 \leq \phi_{\rm orb} \leq 0.30$ (Fig. 13cef). Its amplitude increases to $A_1 = 0.^{\rm m}154$

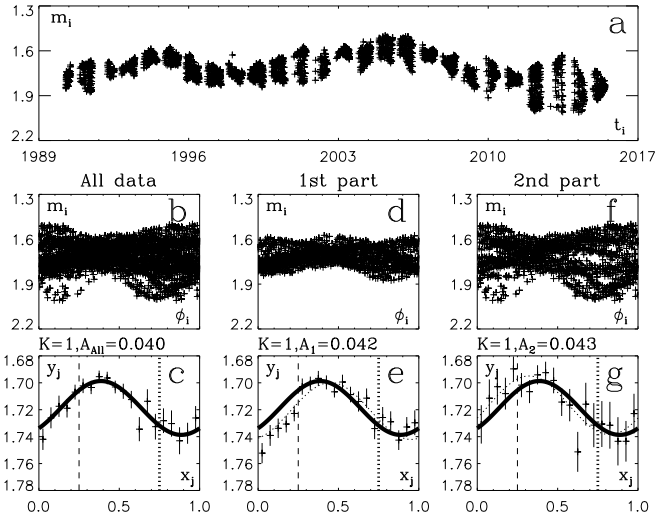

Figure 10. BM CVn, otherwise as in Fig. 1.

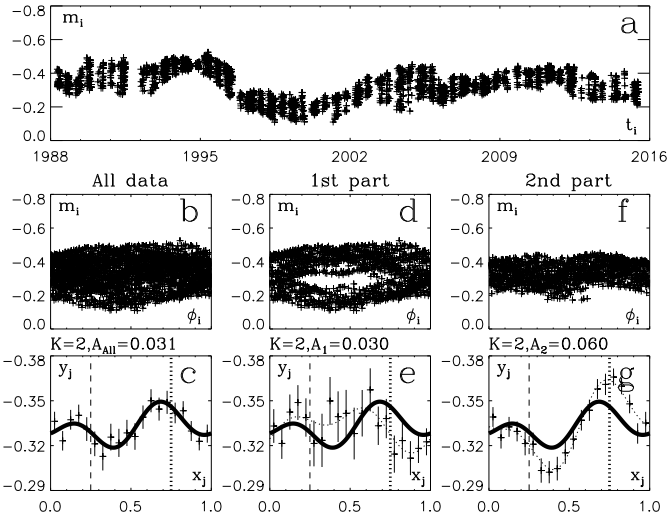

Figure 12. V1762 Cyg , otherwise as in Fig. 1.

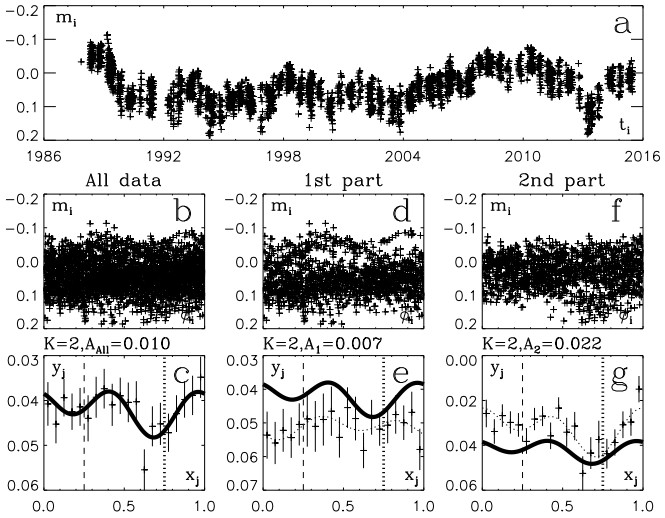

Figure 11. V478 Lyr, otherwise as in Fig. 1.

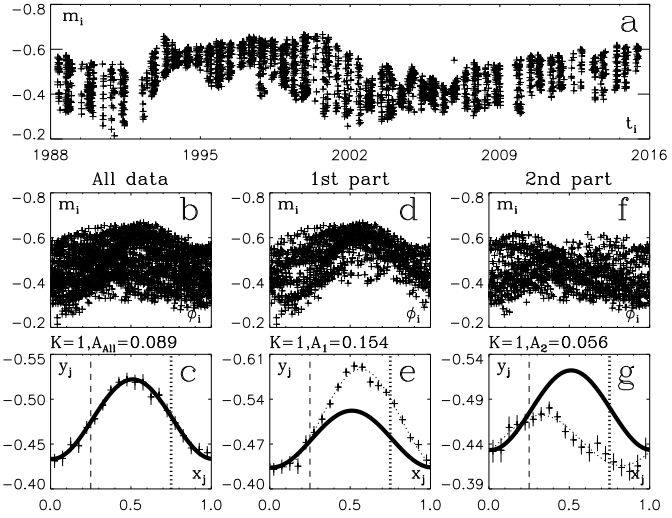

Figure 13. HK Lac , otherwise as in Fig. 1.

during the 1st part of data and decreases to $A_2 = 0.^{\rm m}056$ during the 2nd part. MLC minimum and shape remain nearly unchanged. Epochs Ac and Aa coincide with MLC maxima and minima in Fig. 13g during the 2nd part of data (Koen & Eyer 2002; Gorza & Heard 1971; Özeren et al. 1999; Cardini 2005, $P_{\rm orb}$, t_0, e, Sp-type of member A).

4.14. *MLC of II Peg*

II Peg has a sinusoidal MLC with a relatively large amplitude, $A_{\rm All} =^{\rm m} 0.064$ (Fig. 14c). The amplitude is $A_1 = 0.^{\rm m}088$ in the 1st part of data, and then increases to $A_2 = 0.^{\rm m}121$ in the 2nd part. MLC minimum and maximum phases are close to Ac and Aa in Fig. 14c, but they shift $\Delta\phi_{\rm orb} = -0.2$ backwards in the 1st part, and then return back to phases $\phi_{\rm orb} = 0.3$ and 0.8 in the 2nd part (Berdyugina et al. 1998, $P_{\rm orb}$, t_0, e, Sp-type of member A).

5. CPS ANALYSIS RESULTS

Next, we apply the Continuous Period Search (Lehtinen et al. 2011, hereafter CPS) to the differential V magnitudes of our 14 CABS. This gives us the following light curve parameters

$M_{\rm CPS}(\tau_{\rm CPS})$ = Mean

$A_{\rm CPS}(\tau_{\rm CPS})$ = Peak to peak amplitude

$P_{\rm CPS}(\tau_{\rm CPS})$ = Period

$t_{\rm CPS,min,1}(\tau_{\rm CPS})$ = Primary minimum epoch

$t_{\rm CPS,tmin,2}(\tau_{\rm CPS})$ = Secondary minimum epoch

where $\tau_{\rm CPS}$ is the mean of all observing times t_i of y_i of the modelled dataset. Lehtinen et al. (2011) formulated this method. It has been applied to the photometry numerous stars (e.g. Hackman et al. 2011; Kajatkari et al.

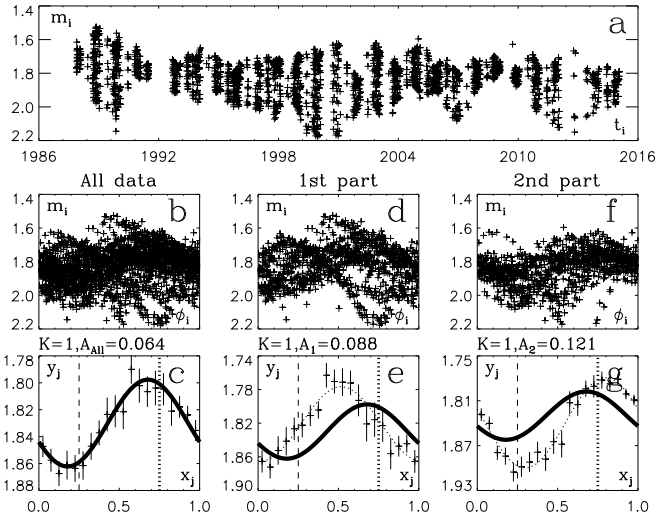

Figure 14. II Peg, otherwise as in Fig. 1.

Table 3
Active longitude.

Variable	n	$P_{\rm act}$ [d]	$Q_{\rm K}$	$t_{\rm cyc,0}$ [HJD]	$P_{\rm cyc}$ [d]	$P_{\rm cyc}$ [y]
DM UMa	54	7.4898 ± 0.0008	$3\text{x}10^{-11}$	47499.990	25506	69.8
XX Tri	59	23.77 ± 0.01	$2\text{x}10^{-11}$	48237.800	2860	7.8
EL Eri	19	47.69 ± 0.02	0.0006	49236.206	4017	11.0
V711 Tau	70	2.8924 ± 0.0002	0.003	47171.961	126	0.3
EI Eri	24	1.9545 ± 0.0008	0.008	47453.341	527	1.4
V1149 Ori	26	53.14 ± 0.06	0.02	47467.507	6550	17.9
σ Gem	97	19.497 ± 0.005	$2\text{x}10^{-8}$	47166.728	3557	9.7
FG Uma	91	21.12 ± 0.01	$2\text{x}10^{-6}$	48706.889	1883	5.2
HU Vir	74	10.419 ± 0.001	$1\text{x}10^{-8}$	48355.411	3438	9.4
BM CVn	93	20.513 ± 0.006	$1\text{x}10^{-6}$	47989.696	3771	10.3
V1762 Cyg	64	28.17 ± 0.02	0.0002	47284.236	1919	5.3
HK Lac	67	24.40 ± 0.01	$4\text{x}10^{-9}$	47299.669	20988	57.5
II Peg	77	6.7119 ± 0.0007	$8\text{x}10^{-8}$	47122.096	3667	10.0

Note. — Variable (Col 1), Number of $t_{\rm CPS,min,1}$ estimates (Col 2: n), Active longitude period and its critical level (Cols 2 and 3: $P_{\rm act}$, $Q_{\rm K}$), Lowest $t_{\rm CPS,min,1}$ value (Col 4: $[t_{\rm cyc,0}]$)), Lap cycle period of Eq. 4 (Cols 5 and 6: $[P_{\rm cyc}]$)

2014; Lehtinen et al. 2016) and it is therefore not described here in greater detail. We use only the results for independent and reliable datasets. "Independent" means that the modelled datasets do not overlap, i.e. they have no common y_i values. The meaning of "reliable" is that all model parameters, e.g. the residuals of the model, have a Gaussian distribution. The interesting parameters for the current study are only $A_{\rm CPS}$ and $t_{\rm CPS,min,1}$, because Fig. 1–27 are in particularly connected to the changes of these two parameters. In other words, the periods $P_{\rm orb}$ in Fig. 1-14 are constant, while Figs. 15 and 27 show only the changes of $A_{\rm CPS}$ and $t_{\rm CPS,min,1}$. The number of estimates obtained for these parameters are given Table 3. Very few reliable estimates are obtained for V478 Lyr ($n = 6$), because its photometric rotation period is so close to 2.1 days. It is difficult to get an adequate phase coverage within 30 days before its light curve changes. Therefore, the analysis of this CABS stops here.

We apply the non–weighted Kuiper test formulated in Jetsu & Pelt (1996) to the primary minima $t_{\rm CPS,min,1}$ of the remaining thirteen CABS. The tested period interval is ± 15 % at both sides of $P_{\rm orb}$. The results for the active longitude periods ($P_{\rm act}$) and their critical levels ($Q_{\rm K}$) (Jetsu & Pelt 1996, their Eq. 24) are given in Table 3. The critical ($Q_{\rm K}$) levels are significant, i.e. active longitudes definitely represent a real dominant phenomenon in these CABS. The active longitudes of V1149 Ori have the lowest significance ($Q_{\rm K} = 0.02$).

We define a lap cycle period

$$P_{\rm cyc} = |[P_{\rm orb}^{-1} - P_{\rm act}^{-1}]^{-1}|, \quad (4)$$

which is the time interval when the difference in completed rounds is one round more or less for the periods $P_{\rm orb}$ and $P_{\rm act}$. We use the absolute value of $P_{\rm cyg}$, because $P_{\rm orb} > P_{\rm act}$ gives a negative $P_{\rm cyc}$ value. The active longitudes in these CABS can rotate faster or slower than orbital motion (Table 3, or compare Figs. 21 and 23). The phases are

$$\phi_{\rm act} = {\rm FRAC}[(t - t_{\rm cyc,0})/P_{\rm act}]. \quad (5)$$

where $t_{\rm cyc,0}$ is the first $t_{\rm CPS,min,1}$ value of each CABS given in Table 3. The lap cycle phases are

$$\phi_{\rm cyc} = {\rm FRAC}[(t - t_{\rm cyc,0})/P_{\rm cyc}]. \quad (6)$$

We compute the binned $A_{\rm cyc,binned}(\phi_{\rm cyc})$ values of all $A_{\rm CPS}$ amplitudes with respect to this phase. The standard deviations of these binned amplitudes within each bin, $S_{\rm cyc,binned}(\phi_{\rm cyc})$, are also computed. These standard deviations measure the scatter of $A_{\rm CPS}$ values within each bin. We use only eight bins, because the total number of $A_{\rm CPS}$ estimates is low, typically about fifty values. We also compute the binned $A_{\rm orb,binned}(\phi_{\rm orb})$ values with respect to the orbital phase $\phi_{\rm orb}$, as well as the standard deviations $S_{\rm orb,binned}(\phi_{\rm orb})$. The scatter can not be large for amplitudes very close to zero, and this may introduce some bias in the interpretation of $S_{\rm cyc,binned}$ and $S_{\rm orb,binned}$ changes. The results for our thirteen CABS are shown in Figs. 15 – 27.

5.1. *Active longitudes and amplitudes of DM UMa*

The lap cycle of DM UMa is surprisingly long, $P_{\rm cyc} = 69.8$ years! The regular migration of the $t_{\rm CPS,min,1}$ phases becomes irregular when the active longitude crosses the orbital period phase $\phi_{\rm orb} = 0.75$ (Fig. 15a: crossing continuous and dotted lines). The gap with no data in Fig. 15b awaits for the missing future observations. The connection $A_{\rm CPS}$ to $\phi_{\rm orb}$ is not clear (Figs. 15b). We get only four binned $A_{\rm cyc,binned}(\phi_{\rm cyc})$ and $S_{\rm cyc,A}(\phi_{\rm cyc})$ values (Figs. 15cd). The seven $A_{\rm orb,binned}$ values (Fig. 15f) show a regular connection to $\phi_{\rm orb}$ which is confirmed by the $S_{\rm orb,binned}$ changes (Figs. 15g).

5.2. *Active longitudes and amplitudes of XX Tri*

The lap cycle of XX Tri is $P_{\rm cyc} = 7.8$ years. It is clearly not the cycle of the mean brightness (Fig. 2a). The active longitude is very stable (Fig. 16a). There are some migration irregularities, especially when the active longitude migrates across orbital phases $\phi_{\rm orb} = 0.25$ and 0.75. The changes of $A_{\rm CPS}(\phi_{\rm cyc})$ are very regular, as well as those of $A_{\rm cyc,binned}(\phi_{\rm cyc})$ and $S_{\rm cyc,A}(\phi_{\rm cyc})$

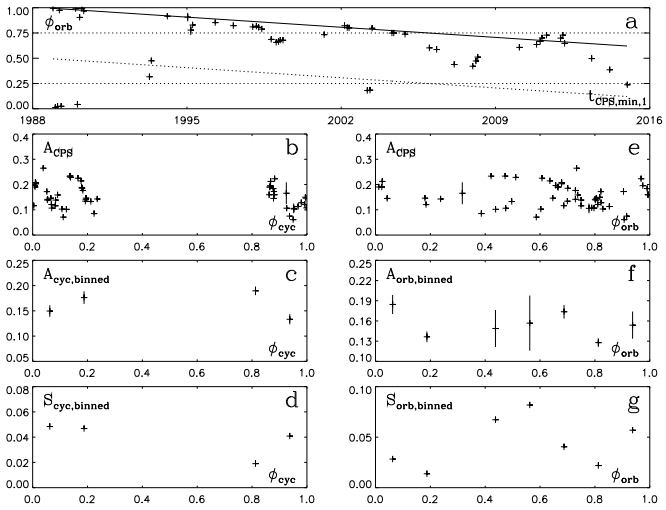

Figure 15. DM UMa. (**a**) Orbital phases ϕ_i for primary minima $t_{\mathrm{CPS,min,1}}$, Orbital phases $\phi_{\mathrm{orb}} = 0.25$ and 0.75 (dotted lines), Active longitude phases $\phi_{\mathrm{orb}} = 0$ (continuous line) and 0.50 (dashed line). (**b**) All amplitudes A_{CPS} versus ϕ_{cyc}, (**c**) Binned amplitudes $A_{\mathrm{CPS,binned}}$ versus ϕ_{cyc}, (**d**) Binned standard deviations $A_{\mathrm{CPS,binned}}$ versus ϕ_{cyc}, (**e**) All amplitudes A_{CPS} versus ϕ_{orb}, (**f**) Binned amplitudes $A_{\mathrm{CPS,binned}}$ versus ϕ_{orb}, (**g**) Binned standard deviations $A_{\mathrm{CPS,binned}}$ versus ϕ_{orb}

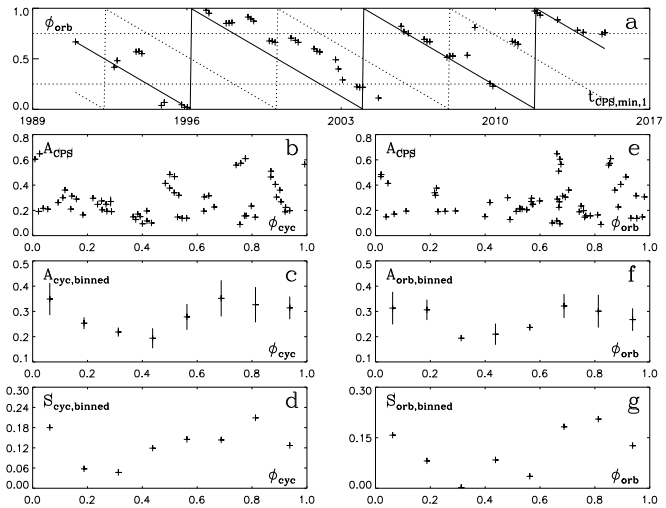

Figure 16. XX Tri, otherwise as in Fig. 15

(Figs. 16bcd). The $A_{\mathrm{CPS}}(\phi_{\mathrm{orb}})$, $A_{\mathrm{orb,binned}}(\phi_{\mathrm{orb}})$ and $S_{\mathrm{orb,A}}(\phi_{\mathrm{orb}})$ changes are also regular (Figs. 16feg).

5.3. *Active longitudes and amplitudes of EL Eri*

Very few $t_{\mathrm{CPS,min,1}}$ and $A_{\mathrm{CPS,min,1}}$ estimates of EL Eri are available ($n = 19$). The active longitude migration in the $t_{\mathrm{CPS,min,1}}$ phases is stable Fig. (17a). Too few $A_{\mathrm{CPS,min,1}}$ are available to confirm the $P_{\mathrm{cyc}} = 10.9$ years lap cycle (Figs. 17b–d). However, some regularity is present in $A_{\mathrm{orb,binned}}$ and $S_{\mathrm{orb,binned}}$ changes (Figs. 17f–g).

5.4. *Active longitudes and amplitudes of V711 Tau*

The P_{cyc} lap cycle of V711 Tau is very short, only 126 days. The predicted migration is so fast that the dashed and continuous lines used for illustrating it would totally cover Fig. 18a, and we therefore show this migration

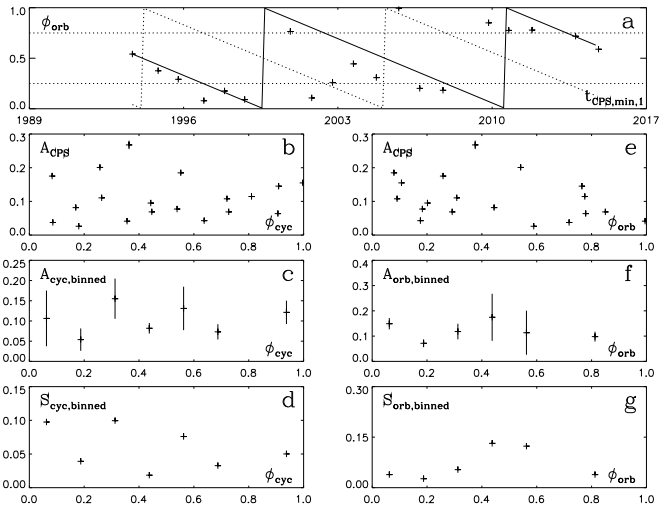

Figure 17. EL Eri, otherwise as in Fig. 15

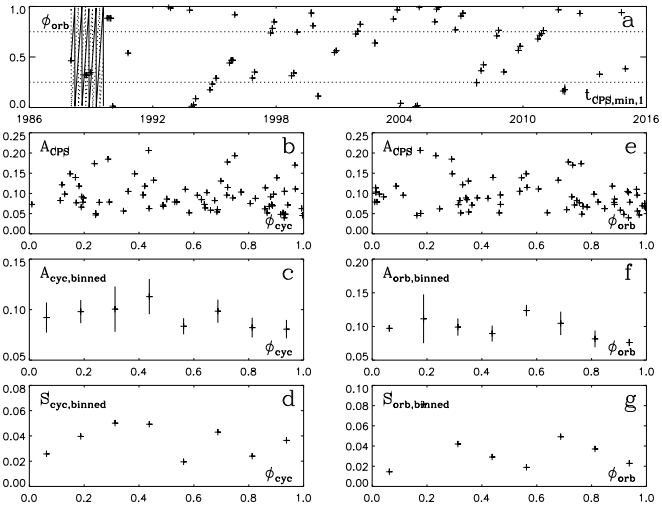

Figure 18. V711 Tau, otherwise as in Fig. 15

only for the first five lap cycles. The $A_{\mathrm{cyc,binned}}$ and $C_{\mathrm{cyc,binned}}$ changes follow the ϕ_{cyc} phases. The connection of $A_{\mathrm{orb,binned}}$ and $S_{\mathrm{orb,binned}}$ to the P_{orb} phases is also excellent.

5.5. *Active longitudes and amplitudes of EI Eri*

The number of $t_{\mathrm{CPS,min,1}}$ and $A_{\mathrm{CPS,min,1}}$ estimates available for EI Eri is only $n = 24$. The migration lines in Fig. 19a are very steep, because the P_{cyc} lap cycle is only 527 days long. Most of the phases of $t_{\mathrm{CPS,min,1}}$ are close to $\phi_{\mathrm{orb}} = 0.25$ and 0.75. The five $A_{\mathrm{cyc,binned}}$, $S_{\mathrm{cyc,binned}}$, $A_{\mathrm{orb,binned}}$ or $S_{\mathrm{orb,binned}}$ estimates can not be used to tell anything about the connection to ϕ_{cyc} or ϕ_{orb}.

5.6. *Active longitudes and amplitudes of V1149 Ori*

The migration of the phases of $t_{\mathrm{CPS,min,1}}$ is very stable for V1149 Ori (Fig. 20a). Two "flip–flop" events occur in the years 1993 and 2000 when the dashed migration line crosses the orbital phase $\phi_{\mathrm{orb}} = 0.25$. Even the connection of *individual* A_{CPS} estimates to ϕ_{cyc} or ϕ_{orb} is regular. The $A_{\mathrm{cyc,binned}}$ and $S_{\mathrm{cyc,binned}}$ changes follow ϕ_{cyc}, and those of $A_{\mathrm{orb,binned}}$ and $S_{\mathrm{orb,binned}}$ follow ϕ_{orb}.

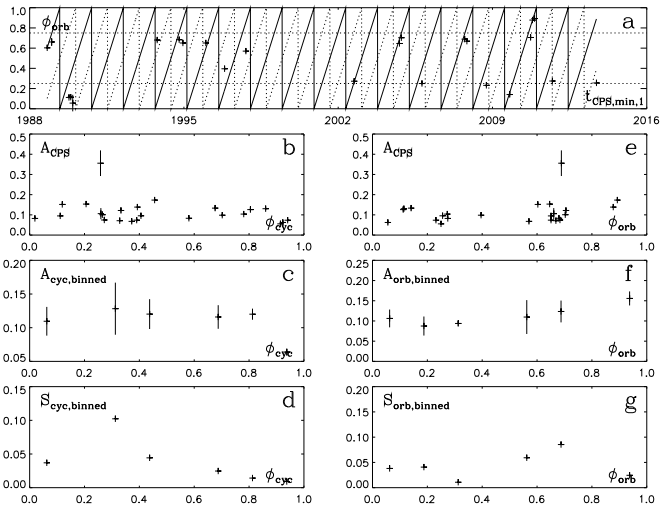

Figure 19. EI Eri, otherwise as in Fig. 15

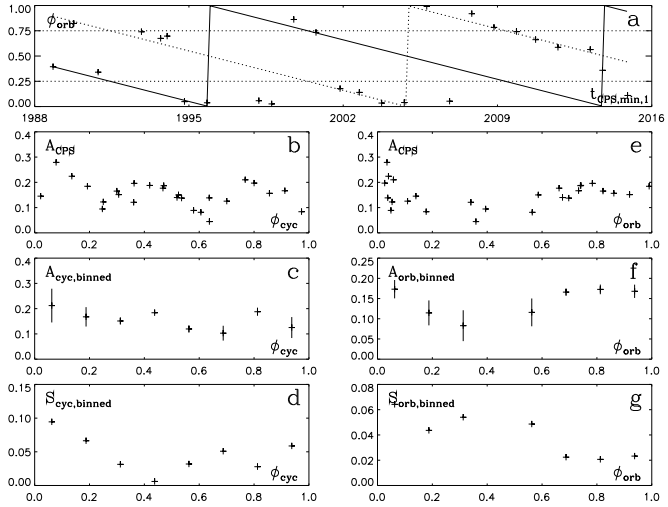

Figure 20. V1149 Ori, otherwise as in Fig. 15

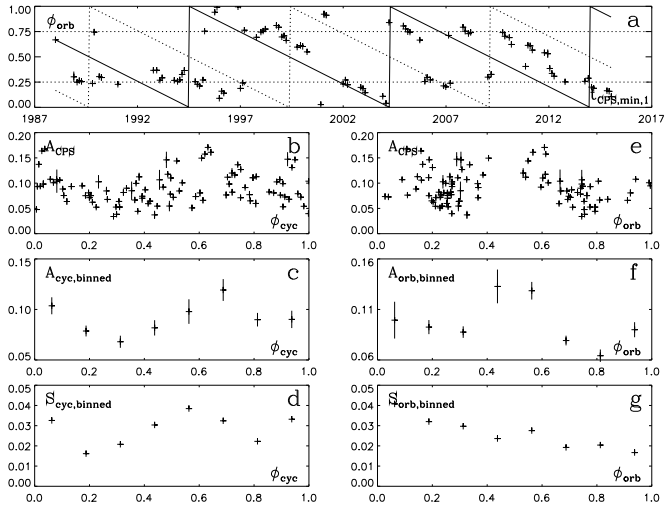

Figure 21. σ Gem, otherwise as in Fig. 15

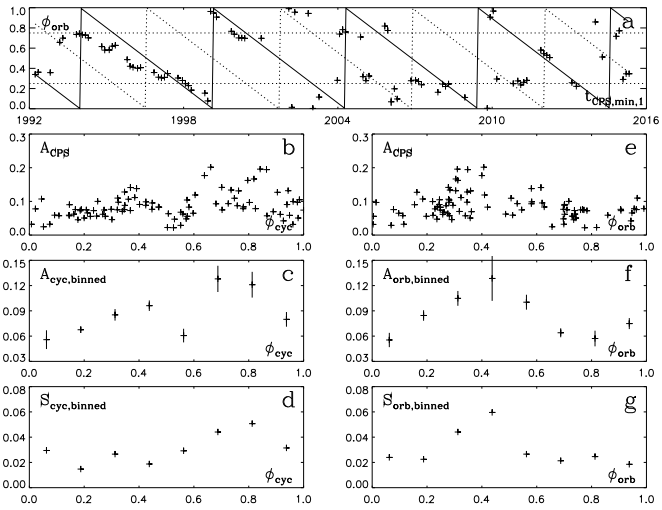

Figure 22. FG UMa, otherwise as in Fig. 15

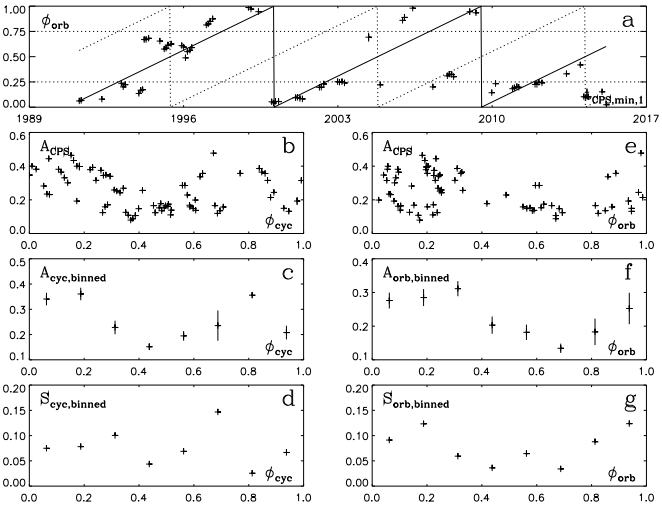

Figure 23. HU Vir, otherwise as in Fig. 15

5.7. *Active longitudes and amplitudes of σ Gem*

How about our favourite star, σ Gem (Jetsu 1996, "Behaves well"). Migration has remained regular (Fig. 21a). Nearly all minima stayed at $\phi_{\rm orb} = 0.25$ before the year 1992, and then they began to migrate downwards. This migration still continues. Four "flip–flop" events occur in the years 1996, 2001, 2005 and 2010. The changes of individual $A_{\rm CPS}$ follow $\phi_{\rm cyc}$ (Fig. 21b). Both $A_{\rm cyc,binned}$ and $S_{\rm cyc,binned}$ follow $\phi_{\rm cyc}$ beyond all ecpectations (Figs. 21cd). Individual $A_{\rm CPS}$ estimates also follow $\phi_{\rm orb}$ and the largest scatter coincides with $\phi_{\rm orb} = 0.25$ and 0.75 (Figs. 21e). Changes of $A_{\rm orb,binned}$ and $S_{\rm orb,binned}$ follow $\phi_{\rm orb}$.

5.8. *Active longitudes and amplitudes of FG UMa*

The migration of FG UMa has been very regular after the "flip–flop" event in the year 1994 (Fig. 22a). The connection of individual $A_{\rm CPS}$ estimates to $\phi_{\rm cyc}$ is clear, as well as that of $A_{\rm cyc,binned}$ and $S_{\rm cyc,binned}$ (Figs. 22bcd). The largest of $A_{\rm CPS}$ scatter coincides with $\phi_{\rm orb} = 0.25$ (Fig. 22e). The $A_{\rm orb,binned}$ and $S_{\rm orb,binned}$ changes are connected to $\phi_{\rm orb}$ (Figs. 22fg).

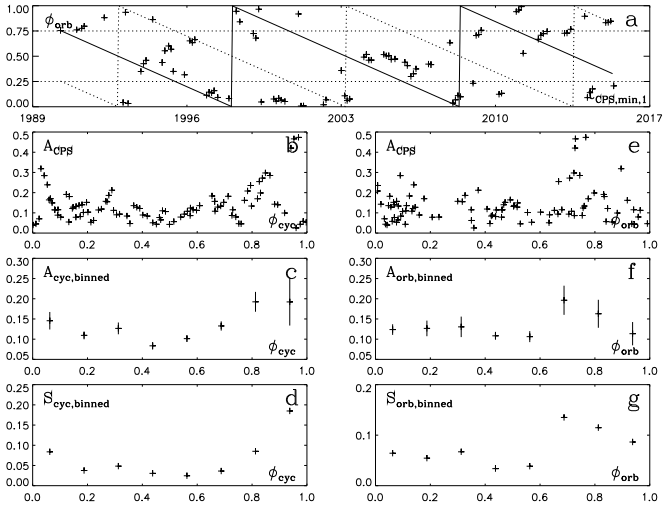

Figure 24. BM CVn, otherwise as in Fig. 15

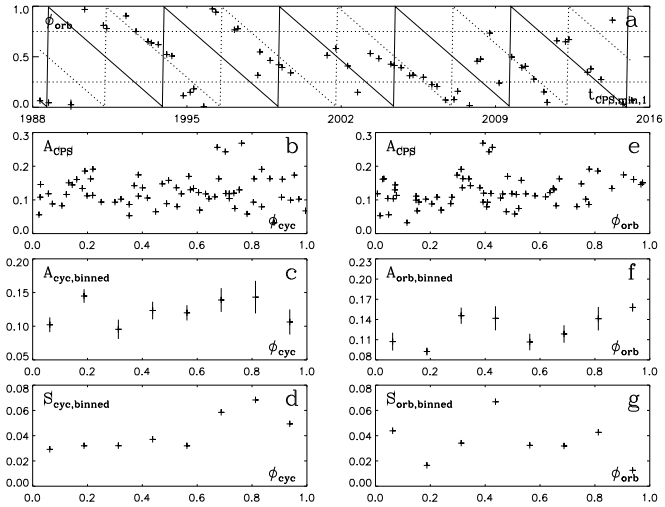

Figure 25. V1762 Cyg, otherwise as in Fig. 15

5.9. *Active longitudes and amplitudes of HU Vir*

A "flip–flop" occured in HU Vir in the year 1994. The light curve minima were at $\phi_{\rm orb} = 0.75$ between the years 1994 and 1997. A shift to $\phi_{\rm orb} = 0.25$ took place in the year 1999, and after that the $t_{\rm CPS,min,1}$ phases have not changed at all (Figs. 23a). Changes of individual $A_{\rm CPS}$ estimates, as well as those of$A_{\rm cyc,binned}$ and $S_{\rm cyc,binned}$, are regular (Figs. 23bcd). The scatter of $A_{\rm CPS}$ is largest at $\phi_{\rm orb} = 0.25$ (Fig. 23e). The connection of $A_{\rm orb,binned}$ and $S_{\rm orb,binned}$ to $\phi_{\rm orb}$ is clear (Figs. 23fg).

5.10. *Active longitudes and amplitudes of BM CVn*

The migration in BM CVn is regular, and "flip–flop" events occur, e.g in the years 1999 and 2009 and 2015 when the continuous line of migration crosses the dotted line at $\phi_{\rm orb} = 0.25$ (Figs. 24a). The changes of individual $A_{\rm CPS}$ estimates display some regularity (Figs. 24b). The connection of $A_{\rm cyc,binned}$ and $S_{\rm cyc,binned}$ to $\phi_{\rm cyc}$ is clear (Figs. 24cd). The largest scatter of $A_{\rm CPS}$ coincides with $\phi_{\rm orb} = 0.75$ (Fig. 24e). The $A_{\rm orb,binned}$ and $S_{\rm orb,binned}$ changes follow $\phi_{\rm orb}$ (Figs. 24fg).

5.11. *Active longitudes and amplitudes of V1762 Cyg*

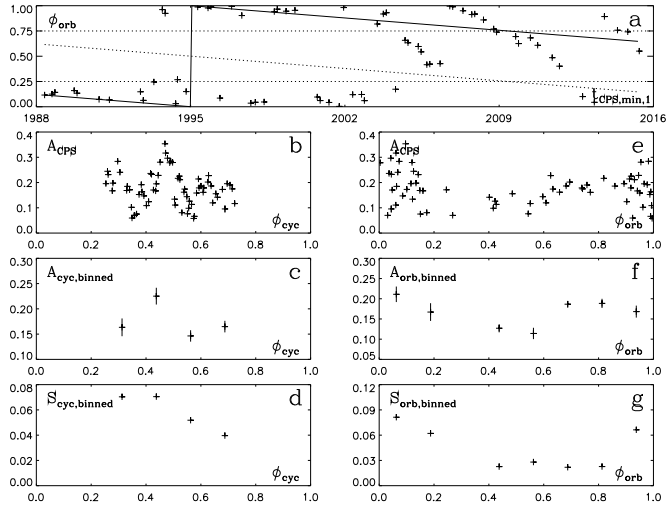

Figure 26. HK Lac, otherwise as in Fig. 15

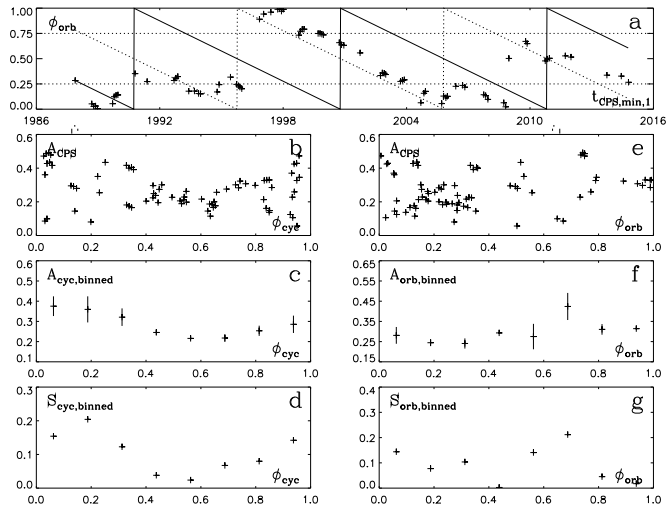

Figure 27. II Peg, otherwise as in Fig. 15

The clearest case of "flip–flop" in V1762 Cyg occurs in 2008 when the continuous line of migration crosses the orbital phase $\phi_{\rm orb} = 0.25$ (Figs. 25a). Individual $A_{\rm CPS}$ change regularly (Figs. 25b). The $A_{\rm cyc,binned}$ and $S_{\rm cyc,binned}$ changes follow $\phi_{\rm cyc}$ (Figs. 25cd). The scatter $A_{\rm CPS}$ is largest at $\phi_{\rm orb} = 0.75$ (Fig. 25e). The $A_{\rm orb,binned}$ and $S_{\rm orb,binned}$ changes are also regular (Figs. 25fg).

5.12. *Active longitudes and amplitudes of HK Lac*

The changes of the light curve minima of HK Lac are exceptional (Figs. 26a). The $t_{\rm CPS,min,1}$ phases remained fixed at $\phi_{\rm orb} = 0.75$ between the years 1988 and 2004. Then linear migration began, and it has continued since then. One "flip–flop" occurs in the year 2007. The long lap cycle period of HK Lac, $P_{\rm cyc} = 57.5$ years, is the reason for the $\phi_{\rm cyc}$ gap with no $A_{\rm CPS}$, $A_{\rm cyc,binned}$ and $S_{\rm cyc,binned}$ estimates in Figs. 26bcd. The largest scatter of $A_{\rm CPS}$ occurs close to $\phi_{\rm orb} = 0.75$ (Fig. 26e). The changes of $A_{\rm orb,binned}$ and $S_{\rm orb,binned}$ are regular (Figs. 25fg).

5.13. *Active longitudes and amplitudes of II Peg*

II Peg is another famous "flip–flop" star (Berdyugina & Tuominen 1998). Our analysis does not reveal a single clear case of "flip–flop" in this CABS (Fig. 27a). The $t_{\rm CPS,min,1}$ phases remained fixed at $\phi_{\rm orb} = 0.25$ between the years 1988 and 1997. Then an extremely regular linear migration began, and it has continued since then. This reveals how subjective the indentifcation of "flip–flop" events can be (e.g. Berdyugina & Tuominen 1998, their Fig. 1). The changes of individual $A_{\rm CPS}$ estimates are not very regular (Figs. 27b), while those of $A_{\rm cyc,binned}$ and $S_{\rm cyc,binned}$ certainly are (Figs. 27cd). The largest scatter of $A_{\rm CPS}$ coincides with $\phi_{\rm orb} = 0.75$ (Figs. 27eg). The changes of $A_{\rm orb,binned}$ and $S_{\rm orb,binned}$ are regular (Figs. 27fg).

6. DISCUSSION

Here, we show that a stationary part of the light curve explains MLC similarities and differences of our fourteen CABS (Sect. 6.1), while a nonstationary part of the light curve explains the active longitudes (Sect. 6.2).

6.1. *Stationary part*

Let us assume that the rotation of member A is synchronized with its orbital motion around member B. In this case, member A always turns the same side towards member B, like the Moon always turns the same side towards the Earth.

In the 1st mode, there is only one spot S1 on A. The brighter side of A is always turned towards B. We observe the maximum projected area of S1 when the line connecting A and B is parallel to our line of sight at epoch Aa. Our notation for this 1st mode is S1f in Fig. 28 (the highest line). MLC minimum coincides with Aa epoch in S1f.

In the 2nd mode, there is again only one spot S1 on A, but the brighter side of A is always turned away from B. The projected area of S1 towards us is largest when the line connecting A and B is parallel to our line of sight at Ac epoch. We denote this 2nd mode as S1b in Fig. 28 (the 2nd highest line). MLC primary minimum coincides with Ac epoch in S1b mode.

There is one larger spot S1 and one smaller spot S2 on A in the 3rd mode. S1 is always turned away from B, and S2 is always turned towards B. We observe the maximum projection of S1 when the line connecting A and B is parallel to our line of sight at epoch Aa. Our notation for this 3rd mode is S12fb in Fig. 28 (3rd highest line). MLC primary minimum coincides with Aa epoch and MLC secondary minimum with Ac in this S12fb mode.

In the last 4th mode, the roles of S1 and S2 spots are reversed, if compared to the 3rd mode, i.e. both spots have shifted by 180 degrees. S1 is always turned towards B and S1 always away from B. We see the largest projected area of S1 at epoch Ac when S2 is out of sight. Our notation for this 4th mode is S12bf in Fig. 28 (2nd lowest line). MLC primary and secondary minima coincide with Ac and Aa in this S12bf mode.

The lowest line of Fig. 28 shows how ellipticity causes two identical MLC minima at Aa and Ac.

The direction of orbital motion is fixed from left (Aa) to right (Ab) in Fig. 28. The results would be same, if this direction were from right to left, because all e values our CABS are zero, or close to zero (Table 1).

Comparison of MLC in Figs. 1 – 14 to Fig. 28 reveals the modes of our fourteen CABS: five in S1f mode (DM UMa, XX Tri, V1149 Ori, BM CVn , HK Lac), two in S1b mode (EL Eri, II Peg), two in S12fb mode (EI Eri, V478 Lyr) and five in S12bf mode (V711 Tau, σ Gem, FG UMa, HU Vir, V1762 Cyg).

The evidence for this "stationary flip–flop" model is overwhelming, as explained in the arguments below.

6.1.1. *Argument 1: Orbital motion connection*

MLC of all data show the orbital phases *where* spots concentrate. MLC of two separate samples of data, like those of the 1st and 2nd part, reveal *where* the largest spot distribution changes take place. The "stationary flip–flop" model explains MLC of all fourteen CABS, especially the connection between orbital phases and MLC primary and secondary minima.

6.1.2. *Argument 2: Mean and amplitude connection*

MLC amplitude decreases when mean brightness increases (e.g. Fig. 2), and it increases when mean brightness decreases (e.g. Fig. 9). Only dark starspots can cause this effect. The longitudinally evenly distributed spots cancel out in MLC, but longitudinally concentrated spots do not. MLC reveals this mean and amplitude connection which fits to the "stationary flip–flop" model. For example, Fig 2 indicates that one side of XX Tri is filled with spots that eventually disappear at the brightness maximum having a low amplitude MLC.

6.1.3. *Argument 3: Single and double peaked MLC connection*

Low and high MLC amplitudes are possible in S1f and S1b modes. However, S12fb and S12bf modes can have only a low amplitude MLC, because the effects of S1 and S2 spots cancel out. This is the reason, why the clearly double peaked MLC have only low $A_{\rm All}$ values (Figs. 4, 5, 7, 8, 11 and 12).

6.1.4. *Argument 4: Ellipticity connection*

The effects of ellipticity can be understood in the context of the "stationary flip–flop" model (Fig. 28: lowest line). Ellipticity can not cause two unequal MLC minima, while spots can. Ellipticity amplifies MLC of S12fb and S12bf modes, but it distorts MLC minima and maxima in S1f and S2b modes, as well as MLC shape. Ellipticity can weaken or strengthen MLC even in the same object, if its modes change. For example, the aforementioned MLC dips of XX Tri (Fig. 2g: $\phi_{\rm orb} \approx 0.25$ and 0.75) and V1762 Cyg (Fig. 6eg: $\phi_{\rm orb} \approx 0.75$) may be an ellipticity effect. In both cases, nearly all spots have faded away, and they do not mask the ellipticity effect.

6.1.5. *Argument 5: "flip–flop" connection*

The four types of "flip–flop" mode changes are

Type I: S1f $\leftrightarrow$ S1b

Type II: S12fb $\leftrightarrow$ S12bf

Type III: S1f $\leftrightarrow$ S12bf

Type IV: S1b $\leftrightarrow$ S12fb

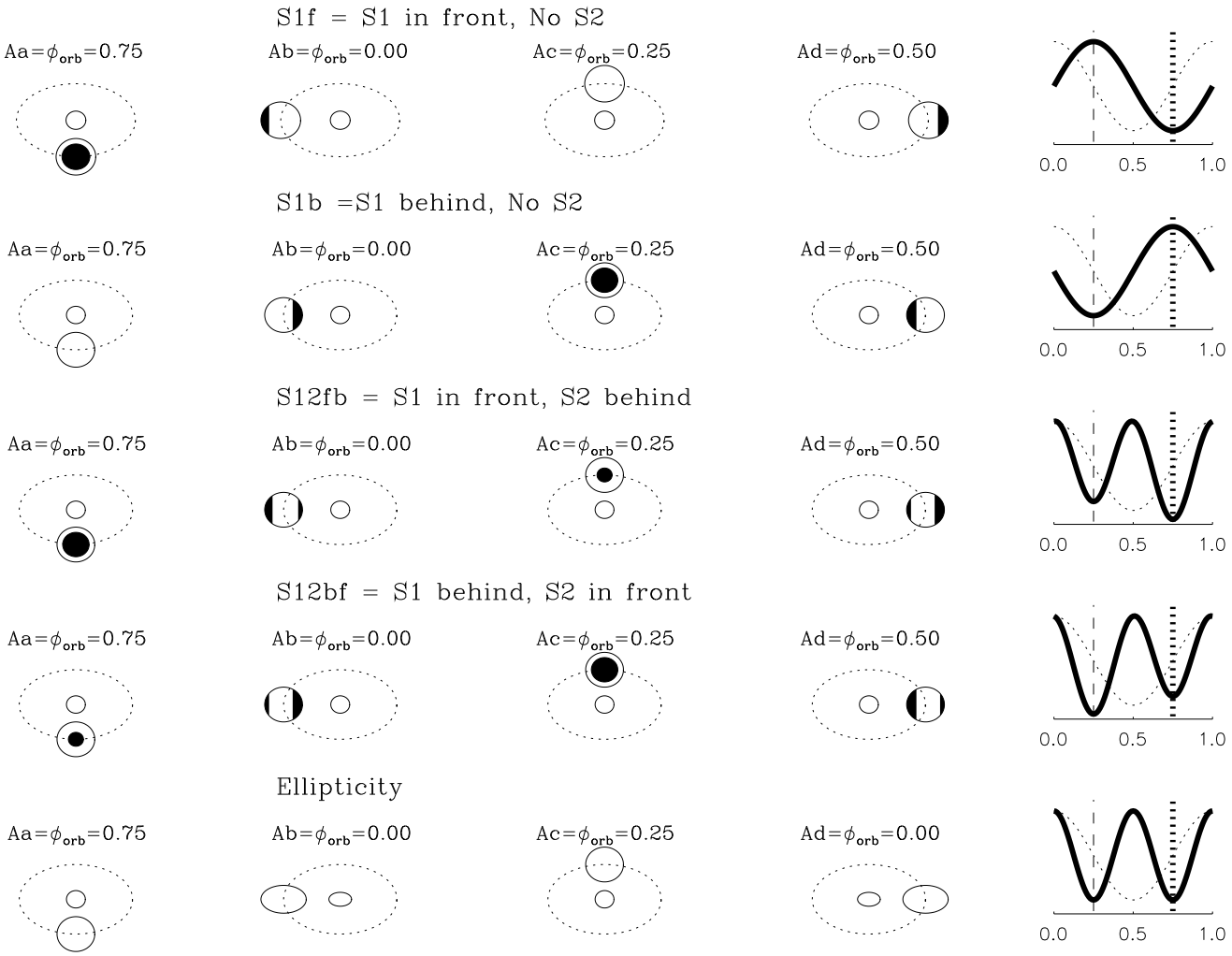

Figure 28. "Stationary "flip–flop"". The highest line: Four first sketches show the S1f mode configuration of CABS at epochs Aa, Ab, Ac and Ad described in Sect. 6.1. The fifth sketch shows the qualitative changes of radial velocity (dashed line) and MLC (thick continuous line) in an arbitrary scale. Vertical lines indicate epochs Aa (thick dotted line) and Ac (thin dashed line). 2nd, 3rd and 4th highest lines: S1b, S12fg and S12bf mode configurations, otherwise as in the highest line. Lowest line: Ellipticy configurations at Aa, Ab, Ac and Ad epoch. Radial velocity and MLC curves are as in the highest line.

The modes may also follow this order

S1f $\leftrightarrow$ S12fb $\leftrightarrow$ S12bf $\leftrightarrow$ S1b.

For example, MLC of EI Eri, V478 Lyr and V1762 Cyg show a Type II "flip–flop" (Figs. 5eg, 11eg and 12eg).

6.1.6. *Some additional arguments*

All starspots of CABS are not circular, like in our "stationary flip–flop" model of Fig. 28. They are not concentrated only on two active longitudes. There are numerous other geometrical and physical phenomena that can induce significant deviations from our simple model. However, considering all these uncertainties, "stationary flip–flop" model works surprisingly well.

The "flip–flop" phenomenon was originally reported in the single G4 giant FK Com (Jetsu et al. 1993). No unique period, like the orbital period of CABS, can be used to compute MLC for single giants like FK Com, or for single main sequence stars like LQ Hya (Lehtinen et al. 2012, K1 V). One solution might be to compute MLC for tested periods within a short interval at both sides of the active longitude period. The tested period with the highest MLC amplitude might reveal similar results as we report here.

All our MLCs are not necessarily representative samples, because we have not observed the full spot cycles of all CABS (e.g. Fig. 2a: XX Tri). It may also be that the "flip–flop" events are connected to spot cycles (e.g. Berdyugina 2005). A sliding window MLC within a time interval shorter than ΔT may reveal such regularities.

Finally, we return back to σ Gem, because the discovery of its ellipticity (Roettenbacher et al. 2015) motivated the current study. This star is a special case, where S1 and S2 nearly equally strong, and even small changes in spot areas can trigger a "flip–flop" events "aided" by the ellipticity effect.

6.2. *Nonstationary part*

The model for the binned MLC data (Eq. 1) is stationary, because the active longitudes are locked to the synchronized orbital motion and rotation frame with the period $P_{\rm orb}$. This model does not explain the regular migration of light curve minima (Figs. 15–27: "a" panels).

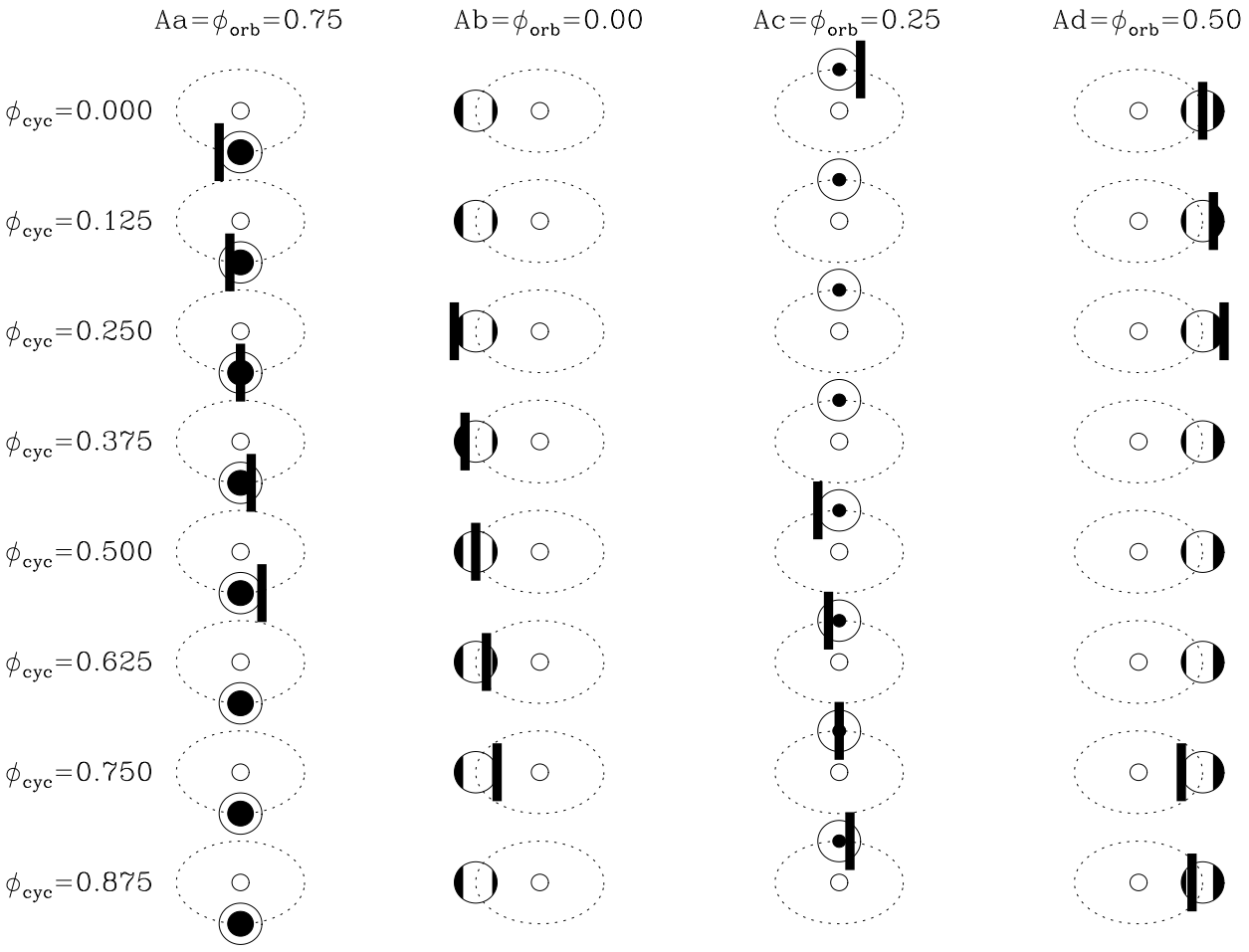

Figure 29. One complete $P_{\rm cyc}$ lap cycle. Lap cycle phases $\phi_{\rm cyc}$ are given on the left of each line. Nonstationary spot S3 (Eq. 7) rotates once around member A during $P_{\rm Cyc}$. Thick dark vertical line denotes the longitude of spot S3 on member A. We mark this longitude only when spot S3 is visible on stellar disk of member A. Locations of stationary spots S1 and S2 (Eq. 8) are as on the third line of Fig. 28.

Such migration has already been reported in binaries and single stars, e.g. by Hackman et al. (2011, II Peg), Kajatkari et al. (2014, σ Gem) or Hackman et al. (2013, FK Com). Our results in Figs. 15–27 show that the CABS light curves contain a nonstationary part

$$f_1(t,\bar{\beta}_1) = M_1 + \sum_{k=1}^{K_2} A_k \cos(\frac{2\pi kt}{P_{\rm act}}) + B_k \sin(\frac{2\pi kt}{P_{\rm act}}) \quad (7)$$

where $\bar{\beta}_1 = [M, A_1, ..., A_{K_1}, B_1, ..., B_{K_1}]$ are the free parameters and $K_2 = 1$ is probably sufficient, because the $t_{\rm CPS,min,1}$ changes have a linear connection to $\phi_{\rm orb}$ (Figs. 15–27: panels "a"). This is the dark longitudinally dominating spot S3 that rotates once around the surface of member A during every $P_{\rm cyc}$ lap cycle (see Fig. 29: dark vertical line). We use a vertical line to denote the longitude of this spot S3, because our figure is already quite crowded by spots S1 and S2. If $f_1(t,\bar{\beta}_1)$ is double peaked, then another nonstationary spot S4 rotates 180 degrees behind S3. For obvious reasons, we have not tried to squeeze spot S4 into Fig. 29.

MLC represent the second stationary part

$$f_2(t,\bar{\beta}_2) = M_2 + \sum_{k=1}^{K_1} C_k \cos(\frac{2\pi kt}{P_{\rm orb}}) + D_k \sin(\frac{2\pi kt}{P_{\rm orb}}) \quad (8)$$

where $\bar{\beta} = [M, C_1, ..., C_{K_1}, C_1, ..., C_{K_1}]$ are the free parameters, and $K_1 = 1$ or 2. We compute the phases $\phi_{\rm orb}$ of this stationary part from the orbital period zero epoch (Table 2: Ab epoch in Eq. 3).

Hence, the suitable CABS light curve model is

$$f(t,\bar{\beta}) = f_1(t,\bar{\beta}_1) + f_2(t,\bar{\beta}_2), \quad (9)$$

where the free parameters M_1 and M_2 are combined to into one free parameter $M = M_1 + M_2$.

This model is linear. The nonstationary $f_1(t,\bar{\beta}_1)$ and stationary $f_2(t,\bar{\beta}_2)$ parts have a unique solution. The interference between these two waves is impossible to foresee without numerical modelling. We will show how the

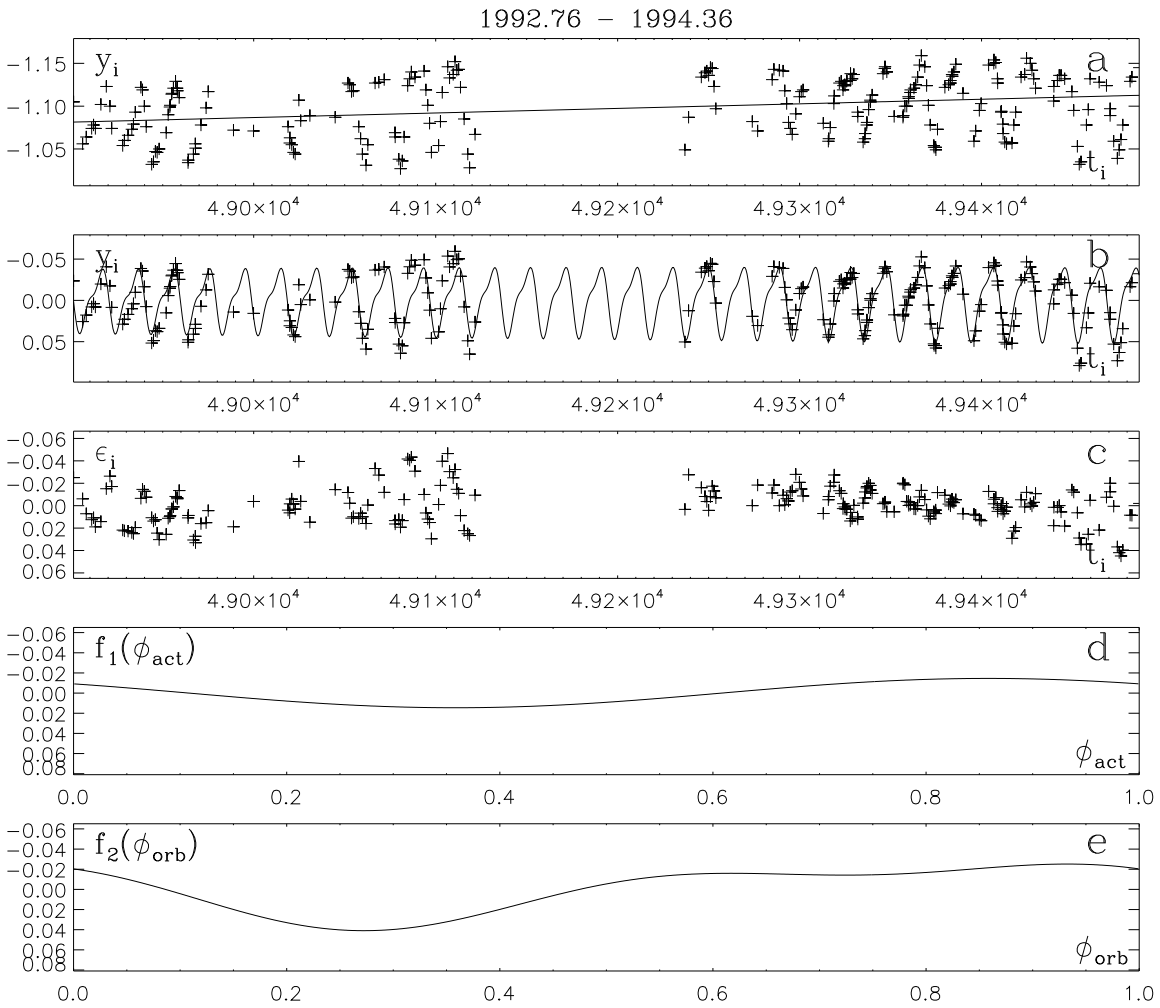

Figure 30. Arbitrary slice of σ Gem photometry. (**a**) Original photometry and a linear fit, (**b**) Original photometry minus linear fit, and model of Eq. 9 ($K_1 = 1, K_2 = 2, M = M_1 = M_2 = 0$), (**c**) Model residuals ϵ_i, (**d**) Nonstationary part $f_1(\phi_{\rm act})$, (**e**) Stationary part $f_2(\phi_{\rm orb})$

model of Eq. 9 explains the four "flip–flop" types of Sect. 6.1.5.

There are striking similarities in Figs. 15-27. The amplitude changes follow both $P_{\rm cyc}$ and $P_{\rm orb}$. This reflects the interference of two "waves" (Eqs. 7 and 8). The "flip–flop" events tend to occur when the active longitudes migrate through phases $\phi_{\rm orb} = 0.25$ and 0.75. The relative strengths of the amplitudes of the stationary part $f_2(t, \bar{\beta}_2)$ and the nonstationary part $f_1(t, \bar{\beta}_1)$ can be reversed at these particular phases. This phenomenon is illustarated in the cases when the minima first follow the horizontal dotted lines and then begin to follow the the tilted continuous or dashed lines, or vice versa (Figs. 15-27 :"a" panels). The two waves can either amplify each other or cancel out at these same phases $\phi_{\rm orb} = 0.25$ and 0.75. Hence, there are numerous reasons for the large scatter of the amplitude values at these two phases. All these regularies allow us to identify the "flip–flop" events nearly unambiguously.

The sketches in Fig. 29 illustrate one $P_{\rm cyc}$ lap cycle. This model works like giant regular clock, where the nonstationary wave rotates once around member A during every lap cycle. The locations of S1 and S2 spots are stable in the synchronized orbital and rotational frame. The sizes and/or temperatures of these spots change. The dramatic events, like "flip–flop" phenomena, are more frequent when spot S3 crosses the longitudes of S1 and S2. If the unseen secondary B member has spots, its stationary spot configuration is most probably similar to that of A member. If this B secondary is a white dwarf, our model predicts its location with respect to S1 an S2 spots on member A. It may now be easier to combine light curves to surface imaging maps (e.g. Hackman et al. 2011; Lindborg et al. 2013), because our model gives the longitudes of spots S1, S2, S3 and S4 at any given epoch in time.

The results for XX Tri reveal that the free parameters of this model of Eq. 9 depend on time, e.g. the mean level of brightness $M = M(t)$. The cycle for the mean of XX Tri (see Fig. 2a) is clearly much longer than the $P_{\rm cyc} = 7.8$ years lap cycle in the light curve amplitude (Table 3). This problem of temporally changing free parameters can be solved by modelling the light curves of Eq. 9 during time intervals (i.e. windows) shorter than the whole time span of the data (ΔT), like with the CPS method (Lehtinen et al. 2011). The information of the long–term evolution of the magnetic fields of CABS is probably coded into the free parameters of this model.

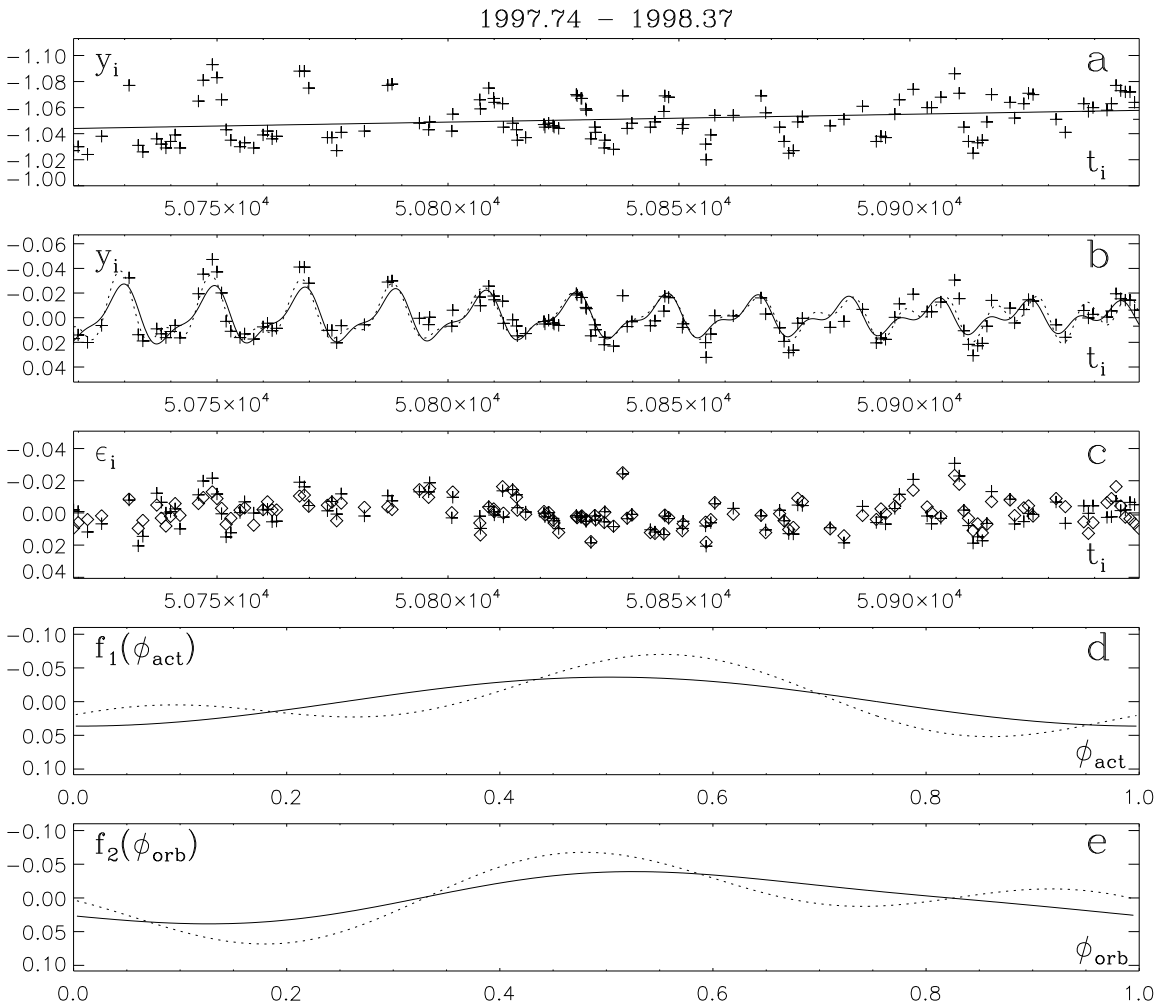

Figure 31. Another slice of σ Gem photometry. (**a**) Original photometry and a linear fit (**b**) Original photometry minus linear fit 1st model (Eq. 9: $K_1 = 1, K_2 = 2, M = M_1 = M_2 = 0$, continuous line) and 2nd model (Eq. 9: $K_1 = 2, K_2 = 2, M = M_1 = M_2 = 0$, dashed line) (**c**) Residuals of 1st model (crosses) and 2nd model (diamonds) (**d**) Nonstationary part $f_1(\phi_{\rm act})$ of 1st and 2nd model (continuous and dashed lines) (**e**) Stationary part $f_2(\phi_{\rm orb})$ of 1st and 2nd model (continuous and dashed lines)

One advantage of our model is that the stationary and nonstationary parts of this magnetic field can be uniquely separated and solved from the light curves.

Here is our short analysis recipe for CABS light curves: *Solve the active longitude period $P_{\rm act}$ from the minima epohcs ($t_{\rm CPS,min,1}$). Use the known orbital period ($P_{\rm orb}$) and apply the model (Eq. 9) to the original photometry.* We show two arbitrary slices of σ Gem photometry in Figs. 30 and 31. The nonstationary and stationary orders of the model for the 1st slice are $K_1 = 1$ and $K_2 = 2$ (Fig. 30). Note that our model gives a unique solution also within gaps of data. Subtraction of the same linear trend from the data at both sides of the gap does not fully eliminate the mean level changes (Figs. 30ab), and the mean residuals are therefore quite large $0.^{\rm m}012$ (Fig. 30c). The two models in Fig. 31b have $K_1 = 1$ and $K_2 = 2$ (continuous line), and $K_1 = 2$ and $K_2 = 2$ (dashed line). Their mean residuals are $0.^{\rm m}007$ (Fig. 31c: crosses) and $0.^{\rm m}006$ (Fig. 31c: diamonds). These values are comparable to the accuracy of our data, $0.^{\rm m}006$. Comparison of Figs. 30de and 31de shows that the nonstationary part, $f_1(\phi_{\rm act})$, and stationary part, $f_2(\phi_{\rm orb})$, of this CABS are indeed changing. The residuals of our model indicate that if the drift of short–lived spots is present in σ Gem, this effect is weak. Although the presence of surface differential rotation is not observed in the movement of starspots of σ Gem, this does not prove that surface differential rotation is absent. However, the stationary and nonstationary spots in σ Gem seem to defy differential rotation.

We give a slightly different recipe for single stars, because they have no $P_{\rm orb}$ value: *Solve the active longitude period $P_{\rm act}$ from the minima epochs ($t_{\rm CPS,min,1}$). Rename $P_{\rm orb}$ to $P_{\rm single}$ in Eq. 8. Test a period interval ± 15 % at both sides of $P_{\rm act}$. Fit our linear model (Eq. 9) with each tested $P_{\rm single}$ value to the original photometry. The $P_{\rm single}$ value that gives the best fit to the data is the rotation period of this single star.* A suitable test statistic is $z_{\rm test} = \sqrt{(1/n)\sum_{i=1}^{n} \epsilon_i^2}$, where ϵ_i are the residuals of the model of Eq. 9 with the known $P_{\rm act}$ value and the tested $P_{\rm single}$ value. This $z_{\rm test}$ is the mean of $|\epsilon_i|$ of each tested model. We tested this method to the single star FK Com using $P_{\rm act} = 2.401151$ to a short slice of photometry from Hackman et al. (2013). A linear fit to these data is shown in Fig. 32a. This linear trend was removed from the data before computing the $z_{\rm test}$ peri-

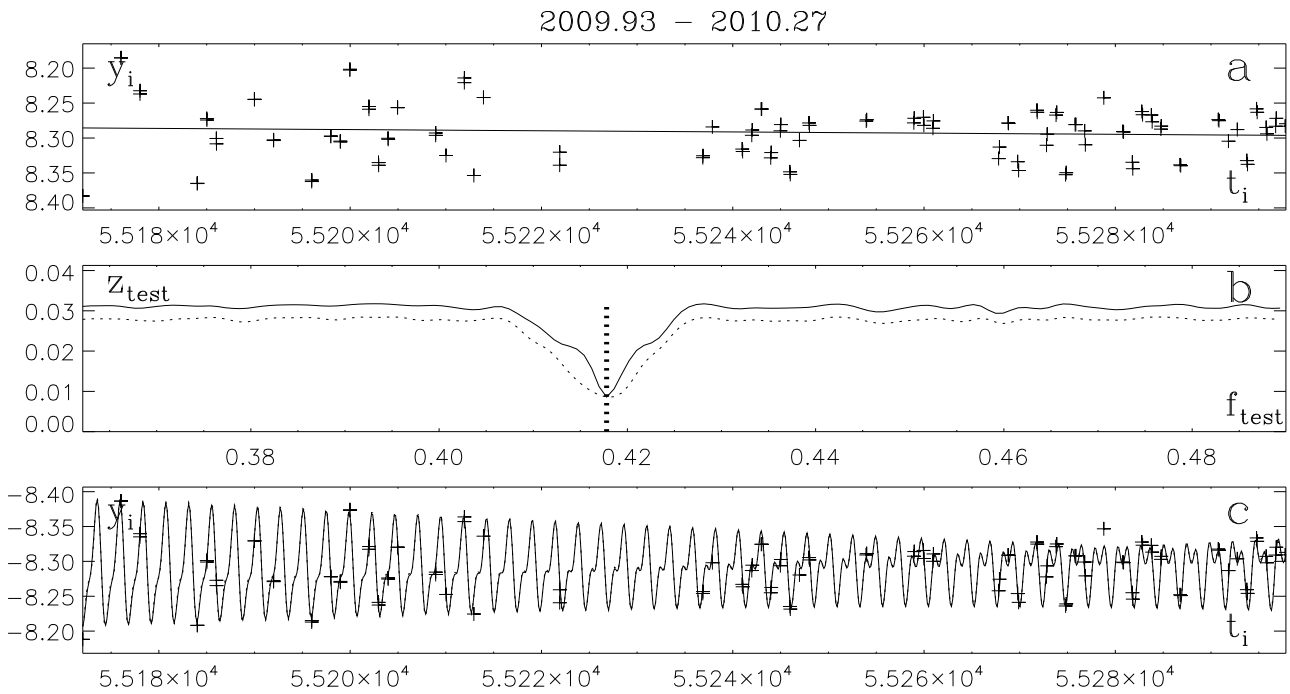

Figure 32. A slice of FK Com photometry. (**a**) Original photometry and a linear fit (**b**) $z_{\rm test}(f_{\rm test})$ periodograms for 1st model (Eq. 9: $K_1 = 1, K_2 = 2, M = M_1 = M_2 = 0, P_{\rm act} = 2.401151$: continuous line), and 2nd model (Eq. 9: $K_1 = 2, K_2 = 2, M = M_1 = M_2 = 0, P_{\rm act} = 2.401151$: dashed line) and best period $P_{\rm single} = 2.3935$ (vertical thick dashed line) (**c**) Respective light curves of the above two models with $P_{\rm single} = 2.3935$: continuous and dashed line.

odograms. We show the periodograms for two models (Eq. 9: $K_1 = 1, K_2 = 2$) and (Eq. 9: $K_1 = 2, K_2 = 2$) in Fig. 32b. The best value was $P_{\rm single} = 2.3935$. The two solutions for the light curve of FK Com overlap in Fig. 32c, because their maximum difference is $0.^{\rm m}006$. The mean residuals of these models are $0.^{\rm m}009$ and $0.^{\rm m}008$. The $P_{\rm act}$ period of FK Com was determined from the light curve minima, like in our CABS analysis. Hence, it represents the nonstationary spot S3 detached from the $P_{\rm single}$ rotation frame of FK Com. Refinement of $P_{\rm act}$ can *only* be achieved from an analysis of new $t_{\rm CPS,min,1}$ data. Our $P_{\rm single} = 2.3935$ value represents the stationary part attached to the rotation frame of FK Com. This value is certainly not final, because different slices of photometry from Hackman et al. (2013) gave different values. A lot of data must be analysed using a much more careful subtraction of the changes of the mean level. We are confident of that this $P_{\rm single}$ value converges to an extremely accurate final value, just like the orbital periods $P_{\rm orb}$ of a binary stars (or the rotation periods of a single stars). Such a result is self evident, because both members of all our CABS have $P_{\rm orb} = P_{\rm single}$. When the two stars in FK Com coalesced, their $P_{\rm orb}$ became $P_{\rm single}$, or equivalently, $P_{\rm orb}$ became meaningless. We emphasize that the $P_{\rm act}$ value of FK Com is already known, but more work is required to determine its $P_{\rm single}$ value. This is one of the advantages of our model: the rotation periods of single active stars are no longer based on the observed changing $P_{\rm phot}$ values (Fig 32b: only one clear minimum).

Let us say a few words about the light curve predictability with Eq. 9, for CABS and single active stars. It is a least partly possible to predict the observed light curves changes when the $P_{\rm orb}$ or $P_{\rm single}$, and $P_{\rm act}$ values are known. The light curve minima follow the "lattice" $\phi_{\rm orb} = \phi_{\rm single} = 0.25$ or 0.75, and $\phi_{\rm act} = 0.00$ or 0.5 (Figs. 15-27: "a"panels). The difference $\Delta P_{\rm orb/single-act} = |P_{\rm orb} - P_{\rm act}| = |P_{\rm single} - P_{\rm act}|$ determines the scale of observed light curve period changes. If the nonstationary part $f_1(t, \bar{\beta}_1)$ is weak, then $P_{\rm act}$ is absent, and the observed light curve period is close to $P_{\rm orb}$. The opposite is true, when $f_2(t, \bar{\beta}_1)$ is weak. If $\Delta P_{\rm orb/single-act}$ is small, the observed light curve period changes are small, and vice versa. The observed period changes reflect this difference $\Delta P_{\rm orb/single-act}$ between two constant periods, i.e. not surface differential rotation. One period may dominate over the other one for a long period of time, e.g. in II Peg the stationary $P_{\rm orb}$ dominated between the years 1987 and 1995, and then the nonstationary $P_{\rm act}$ began to dominate and this domination has continued to the year 2015 (Fig. 27a). The case of HK Lac is very similar (Fig. 26a). The $f_1(t, \bar{\beta}_1)$ and $f_2(t, \bar{\beta}_2)$ amplitudes determine the maximum scale for the observed light curve amplitudes. For example, perhaps the observed surface differential rotation in the light curves of slowly rotating stars is not larger, but the ratio $\Delta P/P_{\rm orb}$ probably is. As for another example, if no active longitude is discovered, then only the nonstationary part is present. No swithces between the domination of $f_1(t, \bar{\beta}_1)$ and $f_2(t, \bar{\beta}_2)$ can occur. This reduces the observed period variations (The Sun and other inactive stars?). The results in Lehtinen et al. (2016) indicate that the nonstationary part is absent in young inactive solar–type stars, because no active longitudes ($P_{\rm act}$) are detected.

The periods $P_{\rm orb}$ and $P_{\rm act}$ of these CABS are constant for long periods of time. The observed photometric periods of these stars appear to change, but this is probably caused by the interference of two constant period waves.

Does this then mean that there is no surface differential rotation in these CABS? It has been known for a long time that surface differential rotation in these rapidly rotating stars is weak (e.g. Hall 1991), but no one has ever seriously claimed that surface differential rotation is totally absent. Surface differential rotation may be present in these CABS, but the locations of stationary S1 and S2 spots seem stable, as well the movement of the nonstationary spots S3 and S4. Could the driving mechanism of magnetic fields in these CABS be the rotation of plasma of free charged particles producing stationary and nonstationary magnetic field waves? Spots S1–S4 are simply the signatures of these waves. And where there is a wave, and another wave, there are probably numerous waves. We have discovered only the two strongest waves in these CABS. Could the interference of stationary and nonstationary waves sustain long-lived magnetic fields? If these waves are stronger in rapidly rotating stars late type stars, their interference produces stronger spots. Could interference explain the differences between the magnetic fields of early and late type stars? In early type stars, their radiative envelopes allow the waves of the magnetic field to remain stable. In late type stars, convection complicates things. Thus, quasiperiodic spot distribution changes are observed in late-type stars, and stable spot distributions in early type stars? A more sophisticated version of our model could be a sum of spherical functions describing the stationary and nonstationary magnetic field waves. Perhaps the free parameters of this model could be solved from observations.

This brings us back to the two currently known alternatives for magnetic fields in all spectral types

1. Rotation and convection (dynamo)

2. Fossil fields

We admittedly only speculate about a third alternative

3. Rotation and interference

"Rotation" is present only in two of these three alternatives. Or is "rotation" present in all three alternatives? Our expertise lies in time series analysis, not in the modelling stellar magnetic fields. Therefore, this interference hypothesis of ours is tentative.

Here is our simple analogy. The orbital and rotation periods of the Moon are equal. Due to this synchronization, we never see the dark side of Moon when it is illuminated by the Sun. Imagine that a giant large dark circular screen would begin to rotate around the Moon with a period of for example ten years ($P_{\rm act}$). This is what we see in CABS and single stars. The main differences are that the rotation period of Earth is not synchronized with the orbital motion of the Moon, and the "spot" on the Moon is not stuck to its surface, but moves due to the illumination of the Sun.

7. CONCLUSIONS

We present a general model for the light curves of chromospherically active single and binary stars (Eq. 9). This model explains the connection between orbital motion, long-term starspot distribution changes, ellipticity and "flip–flop" events in CABS. The Ancient Egyptians discovered Algol's regular eclipses. Some day this model of ours is perhaps referred to as something discovered by the Ancient Finns and Americans. The history of mankind pales when compared to the millions or billions of years that these CABS have already spent in synchronous orbital motion and rotation. Two stars A and B are endlessly staring at each other's faces. Spots S3 and S4 (if present) occasionally arrive to meet spots S1 and S2 at every multiple epoch of half lap cycle $P_{\rm cyc}$. Otherwise, this peaceful arrangement is nearly eternal. This idea of "nothing ever happens" is something that truly works in astronomical time scales. The geometry of the magnetic fields in these CABS does in some ways begin to resemble the never changing geometry of the magnetic fields of Ap stars, the oblique rotator model (e.g. Jetsu et al. 1992, CQ Uma). Are we observing interference waves of "Oh Be A Fine Girl. Kiss Me, Right Now or Soon."

This work has made use of the SIMBAD database at CDS, Strasbourg, France and NASA's Astrophysics Data System (ADS) services. The automated astronomy program at Tennessee State University has been supported by NASA, NSF, TSU and the State of Tennessee through the Centers of Excellence program.

REFERENCES

Balona, L. A. 1987, South African Astronomical Observatory Circular, 11, 1
Barrado y Navascues, D., de Castro, E., Fernandez-Figueroa, M. J., Cornide, M., & Garcia Lopez, R. J. 1998, A&A, 337, 739
Berdyugina, S. V. 2005, Living Reviews in Solar Physics, 2, 8
Berdyugina, S. V., Jankov, S., Ilyin, I., Tuominen, I., & Fekel, F. C. 1998, A&A, 334, 863
Berdyugina, S. V., & Tuominen, I. 1998, A&A, 336, L25
Bopp, B. W., & Dempsey, R. C. 1989, PASP, 101, 516
Bopp, B. W., Fekel, F. C., Aufdenberg, J. P., Dempsey, R., & Dadonas, V. 1993, AJ, 106, 2502
Cardini, D. 2005, A&A, 430, 303
Catalano, S., & Rodonò, M. 1967, Mem. Soc. Astron. Italiana, 38, 395
Chugainov, P. F. 1966, Information Bulletin on Variable Stars, 172
Crampton, D., Dobias, J., & Margon, B. 1979, ApJ, 234, 993
Cutispoto, G. 1993, A&AS, 102, 655
—. 1995, A&AS, 111, 507
Donati, J.-F., Brown, S. F., Semel, M., et al. 1992, A&A, 265, 682
Drake, A. J., Graham, M. J., Djorgovski, S. G., et al. 2014, ApJS, 213, 9
Duemmler, R., Ilyin, I. V., & Tuominen, I. 1997, A&AS, 123
Eker, Z., Ak, N. F., Bilir, S., et al. 2008, MNRAS, 389, 1722
Fekel, F. C., & Henry, G. W. 2005, AJ, 129, 1669
Fekel, F. C., Henry, G. W., Eaton, J. A., Sperauskas, J., & Hall, D. S. 2002, AJ, 124, 1064
Fekel, F. C., Moffett, T. J., & Henry, G. W. 1986, ApJS, 60, 551
Fekel, F. C., Quigley, R., Gillies, K., & Africano, J. L. 1987, AJ, 94, 726
Fekel, F. C., Strassmeier, K. G., Weber, M., & Washuettl, A. 1999, A&AS, 137, 369
Fekel, Jr., F. C. 1983, ApJ, 268, 274
García-Alvarez, D., Foing, B. H., Montes, D., et al. 2003, A&A, 397, 285
Glebocki, R., & Stawikowski, A. 1995, Acta Astronomica, 45, 725
Gorza, W. L., & Heard, J. F. 1971, Publications of the David Dunlap Observatory, 3, 99
Griffin, R. F., & Fekel, F. C. 1988, Journal of Astrophysics and Astronomy, 9, 213
Hackman, T., Mantere, M. J., Jetsu, L., et al. 2011, Astronomische Nachrichten, 332, 859

Hackman, T., Pelt, J., Mantere, M. J., et al. 2013, A&A, 553, A40
Hall, D. S. 1972, PASP, 84, 323
Hall, D. S. 1991, in Lecture Notes in Physics, Berlin Springer Verlag, Vol. 380, IAU Colloq. 130: The Sun and Cool Stars. Activity, Magnetism, Dynamos, ed. I. Tuominen, D. Moss, & G. Rüdiger, 353
Hall, D. S., Fekel, F. C., Henry, G. W., & Barksdale, W. S. 1991, AJ, 102, 1808
Hatzes, A. P. 1998, A&A, 330, 541
Henry, G. W. 1999, PASP, 111, 845
Hoffmeister, C. 1965, Veroeffentlichungen der Sternwarte Sonneberg, 6, 97
Jetsu, L. 1996, A&A, 314, 153
Jetsu, L., Kokko, M., & Tuominen, I. 1992, A&A, 265, 547
Jetsu, L., & Pelt, J. 1996, A&AS, 118, 587
Jetsu, L., Pelt, J., & Tuominen, I. 1993, A&A, 278, 449
Jetsu, L., & Porceddu, S. 2015, PLoS ONE, 10
Jetsu, L., Porceddu, S., Lyytinen, J., et al. 2013, ApJ, 773, 1
Kajatkari, P., Hackman, T., Jetsu, L., Lehtinen, J., & Henry, G. W. 2014, A&A, 562, A107
Koen, C., & Eyer, L. 2002, MNRAS, 331, 45
Kron, G. E. 1947, PASP, 59, 261
Lehtinen, J., Jetsu, L., Hackman, T., Kajatkari, P., & Henry, G. W. 2011, A&A, 527, A136
—. 2012, A&A, 542, A38
—. 2016, A&A, 588, A38
Lindborg, M., Mantere, M. J., Olspert, N., et al. 2013, A&A, 559, A97
Osten, R. A., & Saar, S. H. 1998, MNRAS, 295, 257
Özeren, F. F., Doyle, J. G., & Jevremovic, D. 1999, A&A, 350, 635
Porceddu, S., Jetsu, L., Markkanen, T., & Toivari-Viitala, J. 2008, Cambridge Archaeological Journal, 18, 327
Roettenbacher, R. M., Monnier, J. D., Henry, G. W., et al. 2015, ApJ, 807, 23
Samus, N. N., Durlevich, O. V., & Kazarovets, R. V. 1997, Baltic Astronomy, 6, 296
Siltala, L., Jetsu, L., Hackman, T., et al. 2016, ArXiv e-prints
Strassmeier, K. G. 1990, ApJ, 348, 682
—. 1999, A&A, 347, 225
—. 2009, A&A Rev., 17, 251
Strassmeier, K. G., & Olah, K. 1992, A&A, 259, 595
Strassmeier, K. G., Hall, D. S., Eaton, J. A., et al. 1988, A&A, 192, 135